Electrochemistry of Molybdenum Aquo Ions

Thesis by
Mark Thomas Paffett

In Partial Fulfillment of the Requirements
for the Degree of
Doctor of Philosophy

California Institute of Technology
Pasadena, California

1983
(Submitted April 12, 1983)

Acknowledgments

I would like to thank the following professors: Fred Anson, for his patience in dealing with my attempts at scientific writing and often fragmented logic; Harry Gray, for his brilliant simple explanations and for his help in proving that chemistry is most definitely not a sober science; John Bercaw, Bob Grubbs, Terry Collins, and Sunney Chan for their scientific input and social interactions.

I am indebted to my fellow co-workers and peers for their helpful criticism, scientific discussions, general debauchery and many unmentionable acts. The following is a list of those people that have influenced me for any of the above reasons: Jay (Goober) Audett, Steve Rice, Terrance P. Smith, Jeff (Leon) Gelles, Pete (Reefer) Wolczanski, Jimmy Mayer, Greg (Dr. Duck) Hillhouse, Mark (Babs) Thompson, Jay Winkler, Don Nocera, Eric (DM) Moore, John Turner, Steve Cramer, Bruce (the Dinosaur) Clemens, Roger Baar, Dan Buttry, Rich Durand, Carl Murray, Brian Willett, Moses Mares, all other past and present members of Fred Anson's research efforts, all of the assorted members of the AASS, Lee, and Hazel's bar. In addition, the expert typing of Henriette Wymar is greatly appreciated.

Finally, I would like to thank my parents for their general support and my wife, Laurie, and son, Cole, for their enduring patience and inspiration.

Abstract

The electrochemical behavior of selected molybdenum aquo ions in acidic media is examined in relation to solution structure.

The electrochemistry of Mo(VI) in non-complexing aqueous electrolytes is usually severely complicated by the oligomerization and subsequent adsorption of the reactant. This problem can be circumvented by employing dilute ($\leq 10^{-4}$ M) solutions of Mo(VI) in 1 to 2 M trifluoromethanesulfonic acid. Under these conditions staircase voltammograms and pulse polarograms exhibit single, reversible waves that are consistent with the one-electron reduction of an unadsorbed, monomeric Mo(VI) species. The pH dependence of the reduction potentials suggests that two protons are consumed in the reduction of each Mo(VI). The monomeric Mo(V) reduction product undergoes spontaneous dimerization with a rate constant estimated as $10^3 M^{-1} s^{-1}$. It also reduces perchlorate and nitrate anions at a significant rate.

The $Mo_2(V)/Mo_2(III)$ redox couple in acidic solution involves an overall four electron-six proton transfer connecting the two participants. This redox process is characterized by extreme electrochemical irreversibility. Reduction of the $Mo_2(V)$ aquo ion to the $Mo_2(III)$ aquo ion proceeds with αn_a equal to 0.73 and a proton reaction order of 1.4. A chemical step with an inverse dependence on proton concentration precedes the reoxidation of aquo $Mo_2(III)$ to aquo $Mo_2(V)$. Plausible mechanisms are given for these observations.

The trinuclear ions containing Mo(IV), $Mo_3O_4(H_2O)_9^{4+}$ ($Mo_3(IV)$) and an oxalato derivative, $Mo_3O_4(C_2O_4)_3(H_2O)_3^{2-}$, can be reversibly

reduced in acidic media to trinuclear Mo(III) species. The reductions involve two sequential electron transfer steps with formal potentials that are pH dependent:

$$Mo_3(IV) + 2e^- \overset{E_1^f}{\rightleftharpoons} Mo_3(III, III, IV)$$

$$Mo_3(III, III, IV) + 1e^- \overset{E_2^f}{\rightleftharpoons} Mo_3(III).$$

Two waves are evident in voltammograms and polarograms of $Mo_3O_4(C_2O_4)_3(H_2O)_3^{2-}$ but with $Mo_3(IV)$ the two formal potentials are too close together to observe separate waves. However, logarithmic analysis of the shapes of normal pulse polarograms allowed the two formal potentials to be evaluated. The reductions of both complexes are believed to be accompanied by protonation of the bridging and capping oxo-ligands. The new, trinuclear $Mo_3(III)$ species resulting from the three-electron reduction of $Mo_3(IV)$ exhibits a characteristic EPR spectrum. The mixed-valent intermediate, $Mo_3(III, III, IV)$, is diamagnetic. Possible structural changes that accompany the addition of electrons and protons to $Mo_3(IV)$ are discussed.

Table of Contents

CHAPTER 1

The Structure of Aqueous Molybdenum Compounds[1]

Introduction

Molybdenum aquo ions exist in the oxidation states II through VI, and within each distinct oxidation state the coordination environment is quite varied. The structures of these complexes in solution have been addressed by an assortment of physical techniques. The most information has been obtained via two techniques, X-ray diffraction of derivative complexes and extended X-ray absorption fine structure (EXAFS) analysis of the aquo ions themselves. The results of these studies will be briefly reviewed using representative compounds to aid in understanding the electrochemistry and chemical reactivity discussed in later chapters. For comparative purposes, the selected crystal structures will be limited to those with ligands containing predominantly oxygen bound to the central metal atom(s).

X-Ray Crystal Structures of Representative Mo Compounds

Mo(VI)

The synthesis of Mo-containing compounds most often begins with Mo(VI), which in nature usually exists as the tetrahedral anion, MoO_4^{2-}. Below pH 7.0, octahedral coordination prevails as water inserts into the inner coordination sphere. Under certain conditions higher-order oligomers, termed polymolybdates, form.[2] The polymolybdates exist in a multitude of structural types[3] that will not be discussed here. The pertinent structures that Mo(VI) forms in aqueous environments include three distinct types: monomeric, oxo-bridging dimeric, and noninteracting dimeric species.

A short Mo-O multiple bond, designated as the terminal oxo bond,

is present in all three structural types. It arises from the strong σ and π donation of O to the empty d orbitals of Mo(VI). When two or three terminal oxo functionalities are present, the typical cis arrangement dictates optimal multiple bonding to the Mo core. This is seen in the structure[4] of $MoO_2(CH_3COCHCOCH_3)_2$ shown in Figure 1.1A. The terminal oxo bond, hereafter abbreviated as Mo-O_t, has a bond length of 1.71 Å as compared to 1.76 Å found in MoO_4^{2-}. Trans to each Mo-O_t bond are the ligand oxygen atoms at the considerably longer distance of 2.24 Å. The cis ligand oxygen atoms reside at 1.99 Å, again reflecting the trans influence of the strong Mo-O_t bond.

The bonding arguments given for monomeric Mo(VI) are also applicable to the two dimeric structures shown in Figure 1.1B and C. The edta (edta = ethylene diamine tetracetate) complex[5] (Figure 1.1B) contains two noninteracting MoO_3 subunits which are attached to opposite ends of the chelating ligand. The oxo functionalities are also cis to one another and have bond lengths comparable to the monomeric species (1.69 Å). The $Ba[Mo_2O_5(C_2O_4)_2(H_2O)_2]$ structure[6] in Figure 1.1C exhibits a linear Mo-O-Mo bridge with two cis terminal oxo groups on each Mo. The bridge oxygen, O_b, exerts less of a trans influence than the terminal oxo groups and possesses an increased bond length of 1.88 Å.

Mo(V)

The exceptionally short terminal oxo bond that dominates the chemistry of Mo(VI) is also prevalent in Mo(V) structures. In very strong acid Mo(V) exists as the species[7] $MoOX_5^{2-}$ (e.g., X = Cl^-, Br^-, NCS^-). Upon lowering the acidity, dimerization occurs with the

Figure 1.1. A) The structure[4] of $MoO_2(CH_3COCHCOCH_3)_2$,

B) The structure[5] of $Mo_2O_5(C_2O_4)_2(H_2O)_2^{2-}$ in $Ba[Mo_2O_5(C_2O_4)_2(H_2O)_2]$,

C) The structure[6] of $MoO_3(edta)MoO_3$ in $Na_4[MoO_3(edta)MoO_3]^3 \cdot 8H_2O$.

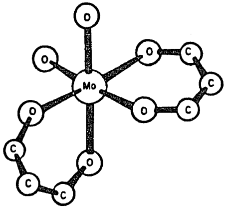
O
O
O
Mo
O
C
C
O
C
O
C
C
C
O

A

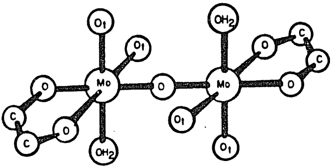
O1
O1
OH2
O
C
C
O
Mo
O
Mo
O
C
C
O
O1
OH2
O1

B

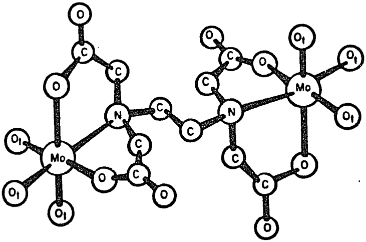
O
C
C
O
N
C
C
O1
Mo
O1
O1
C
O
C
O
O
C
O
C
N
Mo
O1
O1
O1
C
O
C
O

C

initially formed dimer postulated[8] to contain a linear Mo-O-Mo bond. The exact geometrical arrangement of the Mo-O_t bonds is unknown, although an analysis of the bonding isomers by a simple molecular orbital method determined[8] that the two Mo-O_t functionalities must be perpendicular to each other to account for the observed solution paramagnetism. To date, no crystalline derivatives of aqueous Mo(V) complexes possessing a linear oxygen bridge have been obtained with ligands bearing only coordinated oxygen.[7] Lowering the acidity further results in a bonding change in the dimeric core with the usual species obtained from such solutions containing a di-μ-oxo bridge, as exemplified by the structure[9] of $Ba[Mo_2O_4(C_2O_4)(H_2O)_2]$ (Figure 1.2). The significant bond distances are: Mo-Mo 2.56 Å, Mo-O_t 1.70 Å, and Mo-O_b 1.90 Å. It is argued[8] that the observed diamagnetism and close proximity of the two Mo atoms is due to a metal-metal bond, and there is physical evidence[10] to support this idea. The two O_t bonds are cis to each other and, as expected, exert a significant trans influence. The central Mo atoms are situated up out of the plane of the four apical oxygen ligands. In basic solution the cis di-μ-oxo core breaks apart to form a structurally uncharacterized insoluble polymeric molybdenum hydroxide complex.

Mo(IV)

The crystal structures of ions isolated from aqueous solution containing molybdenum in oxidation state (IV) have been determined for anionic complexes containing oxalate[11] and edta[12] as ligands. Both structures are based upon a trimeric core of composition $Mo_3O_4^{4+}$ as shown for $Cs_2[Mo_3O_4(C_2O_4)(H_2O)_3]$ (Figure 1.3). In addition, the

Figure 1.2. The structure[9] of $Mo_2O_4(C_2O_4)_2(H_2O)_2^{2-}$ in $Ba[Mo_2O_4(C_2O_4)_2(H_2O)_2] \cdot 5H_2O$.

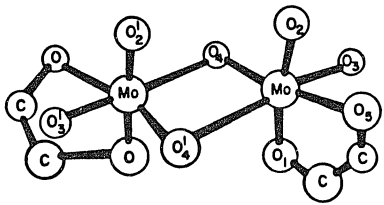
O'2
O
O2
O4
O3
C
Mo
Mo
O'3
O5
C
O
O'4
O1
C
C

Figure 1.3. The structure[11] of $Mo_3O_4(C_2O_4)_3(H_2O)_3^{2-}$ in $Cs_2[Mo_3O_4(C_2O_4)_3(H_2O)_3] \cdot 4H_2O \cdot \frac{1}{2}H_2C_2O_4$.

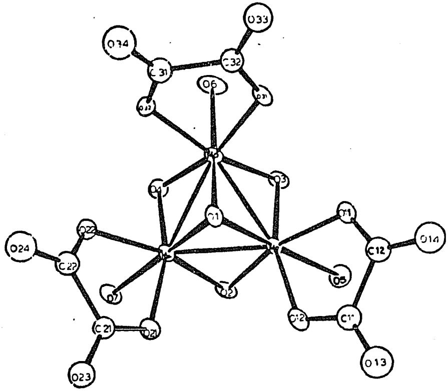
O33
C31
C32
O6
O3
O24
C12
O14
O2
C21
O21
O13
O23

structure of an isothiocyanato complex has been surmised[13] to be trimeric with the same central core composition. The terminal oxo bond, so prevalent in the structures of molybdenum compounds in higher oxidation states, is not present in the trimeric Mo(IV) complexes. Unique to these compounds is the presence of a triply bridging 'capping' oxygen with a Mo-O bond distance of 2.019 Å, longer than that observed for the other bridging oxygen atoms, 1.921 Å. In addition, the Mo-Mo bond distance of 2.49 Å is suggestive of a significant bonding interaction among the three molybdenum centers.

Mo(III)

Structural studies of aqueous Mo(III) complexes are few, presumably due to their sensitivity to molecular oxygen. The aqueous species of interest include monomeric, dimeric, and trimeric aquo ions, of which only the dimeric ion has been characterized structurally[7,14] as a derivative complex. The edta complex of a Mo(III) dimer (Figure 1.4) has been synthesized by reduction of the parent Mo(V) dimer. Noteworthy are the absence of terminally bound oxygen atoms and the presence of a bridging acetate ligand. In addition, the bridging oxygen atoms are protonated and have a Mo-O bond length of 2.04 Å, considerably longer than that found in the Mo(V) dimer. The dihedral angle between the two $Mo(OH)_2$ planes is 166°; the corresponding angle found for the MoO_2 unit in the Mo(V) dimer is 151°. The Mo-Mo distance is 2.43 Å in the Mo_2(III) complex, significantly shorter than in the corresponding Mo(V) dimer.

Mo(II)

To complete the sequence of Mo aquo ions, a discussion of dimeric

Figure 1.4. The structure[14] of $Mo_2(OH)_2(O_2CCH_3)edta^-$ in $K[Mo_2(OH)_2(O_2CCH_3)edta]$.

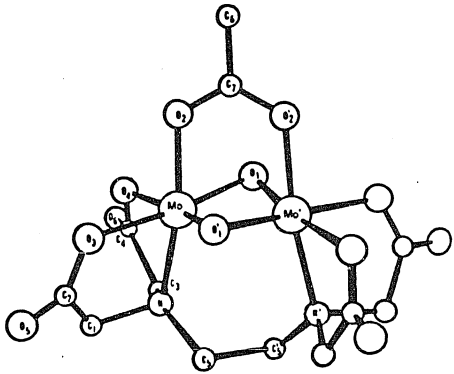
Mo
Mo'

Mo(II) complexes would be useful. The dimeric ions possess short metal-metal distances characteristic of a quadruple bond. For comparison to the following EXAFS studies on the Mo_2^{4+} ion, the structure[15] of $Mo_2(O_2CCH_3)_4$ is shown in Figure 1.5. An exceedingly short Mo-Mo distance of 2.11 Å is found in this well-studied[16] entity. The high symmetry (D_{4h}) is another characteristic feature of dimeric Mo(II) complexes.

EXAFS of Selected Mo Aquo Ions

As a simple aquo ion, molybdenum in the oxidation states II through V is extremely difficult to isolate as a crystalline solid. Although Mo(VI) species are well characterized by X-ray diffraction as simple aquo ions, the other oxidation states are structurally characterized only from derivative complexes. Despite this limitation, a certain knowledge of solution structure has been realized from the EXAFS analysis of selected molybdenum aquo ions.[1] A detailed description of the theory and analysis of EXAFS is beyond the scope of this work; however, for the interested reader several recent reviews[17] are available.

The ability to probe the structure of an ion in solution or of a complex that does not crystallize well is one of the principal strengths of EXAFS studies. The specific information that can be obtained from an EXAFS analysis includes: 1) the distance between the X-ray absorbing and scattering atoms, R_{ab}; 2) the number of backscattering atoms of a particular type, N_b (coordination number); and 3) the root mean square deviation of R_{ab}, σ_{ab} (better known as the Debye-Waller

Figure 1.5. The structure[15] of $Mo_2(O_2CCH_3)_4$.

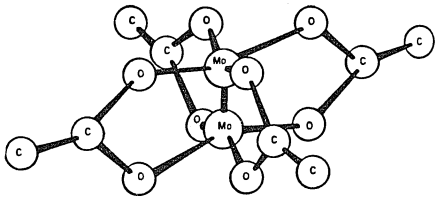
C
C
O
O
C
Mo
O
C
C
O
O
Mo
O
C
C
O
O
C

factor). This information is listed in Table 1.1 for selected molybdenum aquo ions and compounds. Conspiciously absent from Table 1.1 is angular information regarding each absorber-scatterer type. This is a major flaw of the EXAFS technique and limits the analysis to suggesting several possible structures. Nevertheless, from the known crystal structures for each oxidation state and the observed solution chemistry, likely structural candidates for each species can be inferred. The end result of the EXAFS analysis for a variety of aquo ions is shown in Figure 1.6. The specific features of each ion will be discussed in turn.

Mo(V)

The EXAFS spectra of the Mo(V) dimer in acidic solution were analyzed[1] with the following three scattering components: a Mo-Mo distance at 2.56 Å and two separate Mo-O components at 1.68 and 1.93 Å. The scattering amplitudes were compatible with the di-μ-oxo core structure, $Mo_2O_4^{2+}$. The bond lengths for the three components are consistent with those observed in the structure of $Ba[Mo_2O_4(C_2O_4)_2(H_2O)_2]$, mentioned earlier.

Mo(IV)

The EXAFS analysis was done on two Mo(IV) species, solid $K_2[Mo_3O_4(C_2O_4)_3(H_2O)_3]$ and the Mo(IV) aquo ion in 4M CH_3SO_3H. Essentially identical EXAFS spectra were obtained for both species. The scattering amplitude analysis for the oxalate salt produced two Mo-Mo interactions at 2.49 Å, two Mo-O components at 1.88 Å, and four Mo-O′ components at 2.05 ± 0.09 Å. This second shell of oxygen atoms for the oxalate salt is in reasonable accord with the mean

Table 1.1. EXAFS Analysis for Selected Molybdenum Ions

Sample	Component								
	Mo-Mo			Mo-O			Mo-O′		
	N_b	R_{ab} (Å)	σ_{ab} (Å)	N_b	R_{ab} (Å)	σ_{ab} (Å)	N_b	R_{ab} (Å)	σ_{ab} (Å)
Mo(V), 3M HCl(aq)	1	2.56	0.04	2	1.93	0.04	1	1.68	0.04
Mo(IV), 4M CH_3SO_3H (aq)	2	2.49	0.03	2	1.88	0.03	4	2.04	0.08
$K_2[Mo_3O_4(C_2O_4)_3(H_2O)_3]$ [a]	2	2.49	0.03	2	1.91	0.04	4	2.05	0.09
Mo(III), [b] 3M CH_3SO_3H (aq)	1	2.54	0.04	3	2.06	0.04	3	2.20	0.08
Mo(III), [c] 4M CF_3SO_3H (aq)	2	2.49	--	4	2.06	--			
$Mo_3(OH)_4(C_2O_4)_3^-$ [d]	2	2.48	0.05	4	2.03	0.05			
Mo(II), 1M CH_3SO_3H (aq)	1	2.12	0.04	4	2.14	0.10			

a. Solid sample.

b. Dimeric cation (see Chapter 3).

c. Trimeric cation (see Chapter 4).

d. Solid isolated from electrolysis solution (see Chapter 4).

Figure 1.6. Aquo Mo core structures[1] as determined by EXAFS: A) $Mo_2(V)$, B) $Mo_3(IV)$, C) $Mo_3(III)$, D) $Mo_2(III)$, E) $Mo_2(II)$.

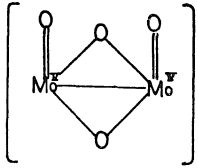

A

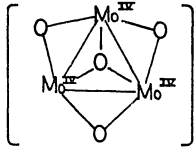

B

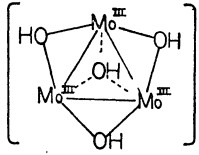

C

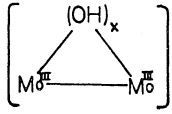

D

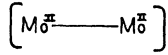

E

distance in the crystal structure of one capping oxygen (μ_3-O) at 2.019 Å, two oxalate oxygens at 2.091 Å, and one coordinated water molecule at 2.154 Å. For the aquo ion the analysis produced two Mo-Mo interactions at 2.49 Å, two Mo-O components at 1.88 Å, and four Mo-O′ components at 2.04 Å. Presumably these second shell oxygen interactions are also a weighted average of capping (μ_3-O) oxygen and coordinated water molecules. Thus, in light of the known structural parameters for $[Mo_3O_4(C_2O_4)_3(H_2O)_3]^{2-}$, the aquo Mo(IV) EXAFS data can be logically interpreted in terms of a trimeric core (Figure 1.6).

In solutions less acidic than 0.01 M H^+ the EXAFS spectra of aquo Mo(IV) display changes that have been attributed[1] to an opening of the trimeric core. In addition, the presence of halide ions had no effect on the EXAFS spectra, suggesting no inner sphere coordination. However, outer sphere ion pairing could occur without any revealing effect on the spectra.

Mo(III)

Two distinct Mo(III) structural types have been examined by EXAFS: the postulated dimeric Mo(III) aquo ion and the Mo(III) ions resulting from reduction of their trimeric Mo(IV) counterparts (see Chapter 4).

The dimeric Mo(III) data were analyzed in terms of one Mo-Mo constituent at 2.54 Å and two different Mo-O interactions, each of coordination number three, at 2.06 and 2.20 Å. The metal-metal distance is clearly longer than that found in the crystal structure of $K[Mo_2(OH)_2(O_2CCH_3)edta]$ and suggests that the acetate ligand influences

the Mo-Mo bonding in the latter compound. The 2.06 Å Mo-O component can be reasonably assigned to bridging hydroxyl groups with the longer Mo-O distance due to coordinated water (it is noteworthy that among the various oxidation states only in the aquo Mo_2(III) species did Mo-OH_2 interactions make a significant contribution to the EXAFS). The analysis clearly rules out an oxo bridged structure for Mo_2(III), although the distinction between a di-μ-OH structure or a tri-μ-OH structure (confacial bioctahedron) is not evident. The second alternative is likely considering the fact that other Mo(III) ions with halide ligands exist with confacial bioctahedral structures[18] (e.g., $Mo_2Cl_9^{2-}$, $Mo_2Br_9^{2-}$).

The EXAFS analysis[19] for the Mo(III) ions resulting from reduction of the Mo(IV) aquo ion and $[Mo_3O_4(C_2O_4)_3(H_2O)_3]^{2-}$ seems consistent with a trimeric formulation. For the aquo ion the Mo-Mo distance of 2.49 Å is preserved and the Mo-O interaction is best fit with average oxygen shell of amplitude $N_b = 4$ at 2.06 Å. In the oxalate ion the Mo-Mo interactions reside at 2.48 Å with the average ($N_b = 4$) Mo-O component at 2.03 Å. No further improvement in the EXAFS curve fitting analysis results by addition of coordinated water to the parameter set. The increased Mo-O components are due to the presence of Mo-OH bridges and are consistent with the observed electrochemistry (Chapter 4).

Mo(II)

The EXAFS spectra of the dimeric Mo(II) ion were analyzed in terms of a single Mo-Mo element at 2.12 Å and four Mo-O interactions at 2.14 Å. The Mo-O distance is reasonable for coordinated water and

is relatively disordered, as judged by the large Debye-Waller factor (0.1 Å). The Mo-Mo bond distance is in excellent accord with that previously discussed for $Mo_2(O_2CCH_3)_4$.

Concluding Remarks

The structural details of the molybdenum aquo ions should facilitate a better understanding of their rich redox behavior and chemical reactivity. In Chapter 2 the electrochemical behavior of MO(VI) in strong acid and the reactivity of a transient Mo(V) monomer toward perchlorate and nitrate reduction will be examined. Chapter 3 addresses the interfacial electron transfer properties of the Mo_2(V)-Mo_2(III) couple with the aim of understanding why this multi-electron redox reaction is so electrochemically irreversible. The electrochemical response of trimeric Mo(IV), with particular regard to the aspects of coupled proton-electron transfer to metal cluster ions, is presented in Chapter 4. The goal of these studies is to achieve a better insight into how molybdenum functions in complex environments, such as supported catalysts, amorphous materials, and metalloenzymes.

References and Notes

1. Portions of this chapter have appeared in print: Cramer, S. P.; Eidem, P. K.; Paffett, M. T.; Winkler, J. R.; Dori, Z.; and Gray, H. B., J. Am. Chem. Soc., 1983, 105, 799.
2. Evans, H. T., Jr., Perspect. Struct. Chem., 1971, 4, 1.
3. Cotton, F. A., and Wilkinson, G., "Advanced Inorganic Chemistry", Wiley, New York, 1972.
4. Kamenar, B. and Penavic, M., Cryst. Struct. Commun., 1973, 2, 41.
5. Park, J. J.; Glick, M. D.; and Hoard, J. L., J. Am. Chem. Soc., 1968, 91, 301.
6. Cotton, F. A.; Morehouse, S. M.; and Wood, J. S., Inorg. Chem., 1964, 3, 1603.
7. Stiefel, E. I., Progr. Inorg. Chem., 1977, 22, 93.
8. Blake, A. B.; Cotton, F. H.; and Wood, J. S., J. Am. Chem. Soc., 1964, 86, 3024.
9. Cotton, F. A.; Morehouse, S. M., Inorg. Chem., 1965, 4, 1377.
10. Winkler, J. R.; Ph.D. Thesis, Caltech, 1984.
11. Bino, A.; Cotton, F. A.; and Dori, Z., J. Am. Chem. Soc., 1978, 100, 5252.
12. Ibid., 1979, 101, 3842.
13. Murmann, K. and Shelton, M., J. Am. Chem. Soc., 1980, 102, 3984.
14. Kneale, G. K.; Geddes, A. J.; Sasaki, Y.; Shibahara, T. and Sykes, A. G., J. Chem. Soc. Chem. Commun., 1975, 356.
15. Lawton, D. and Mason, R., J. Am. Chem. Soc., 1965, 87, 921.

16. Trogler, W. C. and Gray, H. B.; Accts. Chem. Res., 1978, 11, 232.

17. (a) Lee, P. A.; Citrin, P. H.; Eisenberger, P. and Kincaid, B. M.; Rev. Mod. Phys., 1981, 53, 769.
(b) Cramer, S. P.; Hodgson, K. O.; Stiefel, E. I. and Newton, W. E.; J. Am. Chem. Soc., 1978, 100, 2748.

18. Ref. 7, p. 138.

19. Cramer, S. P.; private communication, January 13, 1982.

CHAPTER 2

The Reduction of Mo(VI) in Trifluoromethanesulfonic Acid[1]

Introduction

The electrochemical reduction of aquo molybdenum(VI) has been studied in a variety of supporting electrolytes.[2-6] An early polarographic study[2] in HCl suggested the initial production of a chemically unstable Mo(IV) species while later work by Souchay and co-workers[3,4] proposed that several forms (monomeric, tetrameric, etc.) of Mo(V) were produced and subsequently reduced to Mo(III). A report by Hull[5] indicated that Mo(VI) is reduced in sulphuric acid to produce a Mo(V) species that adsorbs on the electrode but no structures of possible Mo(V) products were proposed. In all of the previous work the voltammetric responses were highly sensitive to the concentration of Mo(VI) and the medium employed. Adsorption on the mercury electrodes was often invoked to account for complex voltammetric behavior, although oligomerization of the variety of molybdenum(VI) oxo-species present in homogeneous solutions has also been suggested.

The objective of the present work was to establish the nature of the initial reduction product of Mo(VI) in a strong noncomplexing electrolyte, trifluoromethanesulfonic acid. It will be shown that low concentrations of Mo(VI) are necessary to suppress adsorption at mercury electrodes and solution oligomerization. In addition, the catalytic reactions of a reduced Mo(VI) species at low concentrations (ca. 5×10^{-5} M) with perchlorate and nitrate ion were monitored in the hope that insight into atom transfer reactions might result.

Experimental

Materials

Trifluoromethanesulfonic acid (Minnesota Mining and Manufacturing Co.) was purified by distillation under Argon. The purified acid was diluted with water and stored in a refrigerator. Reagent grade sodium molybdate was used as received. Ortho-nitroaniline (Aldrich Chemical Co.) was recrystallized twice before use. Solutions were deoxygenated by bubbling with argon or nitrogen that had been passed successively through a solution of V(II) and over hot copper turnings. Solutions were prepared with triply distilled water or distilled water that was further purified by passage through a purification train (Barnstead Nanopure D2790). Solutions were checked for chloride impurities by pulse polarography. Impurity levels in 2M solutions of trifluoromethanesulfonic acid were below 0.1 μM. Stock solutions of Mo(VI) were standardized gravimetrically by precipitation of $PbMoO_4$.[7]

Instrumentation and Techniques

UV spectra were recorded on Cary 17, Varian 219, or Hewlett-Packard 8450 spectrophotometers. Electrochemical experiments were carried out in conventional compartmentalized cells. Experiments at variable temperatures were carried out in a cell with the working electrode compartment jacketed for temperature control. The reference electrode remained at room temperature. Most electrochemical measurements were performed with appropriate combinations of commercially available instruments (Princeton Applied Research Models 173, 174, 175 and 179). The Model 174 Polarographic Analyzer was modified to provide variable pulse width.[8] Cyclic staircase voltammetry

and chronocoulometry were carried out with a computer-based digital data acquisition and analysis system similar to that previously described.[9] Staircase voltammetry[10] was performed with a fixed step height of 4.88 mV. Variation of the effective sweep rate (i.e., [step height] × [step width]$^{-1}$) was obtained by appropriate changes in the step widths. The area of the hanging mercury drop electrodes was 0.032 cm^2. The dropping mercury electrode had a mercury flow rate of 1 to 1.5 mg s^{-1}. Potentials were measured and are quoted with respect to a saturated calomel reference electrode. The Hammett acidities of solutions of CF_3SO_3H between 1 and 4 M were determined from the spectrum of o-nitroaniline indicator in each solution. Digital simulations of staircase voltammograms employed the method of Nicholson and Olmstead.[11] (See Appendix 1 for a listing of the program.)

Results

Voltammograms for the reduction of Mo(VI) in 1.9 M CF_3SO_3H show several distinctive features that depend upon the concentration of Mo(VI) and the length of time that the mercury electrode is exposed to the solution. Figure 2.1 shows a set of cyclic staircase voltammograms for a 0.5 mM solution recorded after various times of exposure. Three reduction peaks are discernible (labeled A, B, and C in Figure 2.1); the most prominent peak appears near -0.5 volt. Plots of peak currents vs. the square root of the effective scan rate (i.e., vs. [step time]$^{-\frac{1}{2}}$) are shown for peaks A and C in Figure 2.2. (Peak B is not well enough resolved at this concentration for a similar analysis.)

Figure 2.1. Cyclic staircase voltammograms of 0.5 mM Mo(VI) in 1.9 M CF_3SO_3H. Before the potential scan the mercury electrode was exposed to the solution for: 1) 0.5, 2) 5.0, 3) 15.0, 4) 45.0 sec. Effective scan rate was 12.2 V s^{-1}.

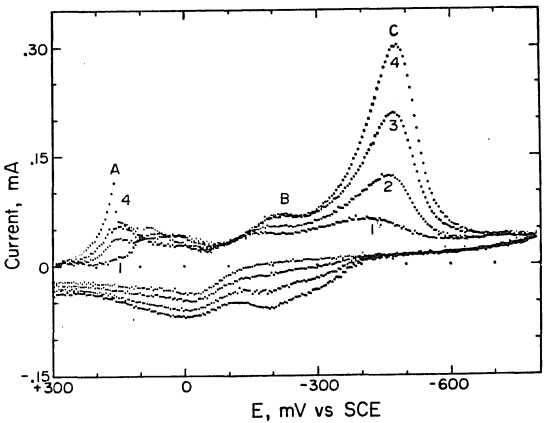
.30
.15
0
-.15
Current, mA
+300
0
-300
-600
E, mV vs SCE
A
B
C
1
2
3
4
4
4

Figure 2.2. Dependence of peak current on (step time)$^{-\frac{1}{2}}$, i.e., (effective scan rate)$^{\frac{1}{2}}$, for peaks A and C of Figure 2.1.

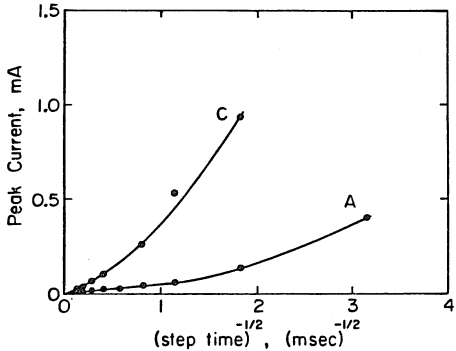
1.5
1.0
0.5
0
Peak Current, mA
C
A
0
1
2
3
4
(step time)^-1/2, (msec)^-1/2

The increasing positive deviations of the peak currents from the expected linear dependence on (step time)$^{-\frac{1}{2}}$ is indicative of strong adsorption of the reactant which also accounts for the otherwise unexpected dependence on electrode exposure time. At concentrations of Mo(VI) of 0.025 mM or less, peak B in Figure 2.1 is better resolved and exhibits a linear dependence of peak current on (step time)$^{-\frac{1}{2}}$. Thus, peak B appears to correspond to the reduction of a diffusing reactant while peaks A and C are dominated by an adsorbed reactant.

At concentrations of Mo(VI) greater than ca. 0.5 mM the voltammetric responses become increasingly complex with obvious evidence of extensive adsorption. A variety of adsorbed species appears to be involved under these conditions which we avoided in order to concentrate on the simpler behavior available with more dilute solutions.

Chronocoulometric Measurement of the Adsorption of Mo(VI).

The extent of adsorption of Mo(VI) was estimated from the intercepts of single step chronocoulometric charge-(time)$^{\frac{1}{2}}$ plots.[12] The double layer charging blank, estimated from identical potential steps in the pure supporting electrolyte, was subtracted from each experimental intercept to obtain the quantity of adsorbed Mo(VI). Adsorption equilibrium was assumed to prevail when continued exposure of the electrode to the solution produced no further changes in the adsorption. Thirty seconds of exposure were usually sufficient for equilibrium to be reached. The results of these measurements are shown in Figure 2.3 for several initial electrode potentials. The most noteworthy feature for present purposes is the sharp decrease in adsorption at concentrations of Mo(VI) near 0.2-0.3 mM. Adsorption of Mo(VI) at

Figure 2.3. Adsorption of Mo(VI) at 0.3 V as a function of the concentration of Mo(VI). The potential was stepped from +0.3 to -0.6 V. Supporting electrolyte: 2 M CF_3SO_3H.

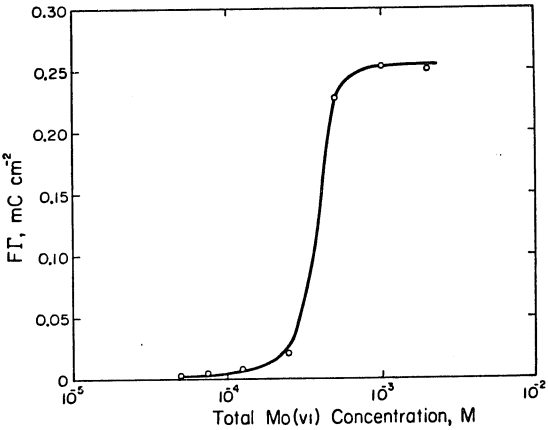
0.30
0.25
0.20
0.15
0.10
0.05
0
FΓ, mC cm⁻²
10⁻⁵
10⁻⁴
10⁻³
10⁻²
Total Mo(vi) Concentration, M

concentrations below ca. 0.1 mM appears to be negligible.

Chemical Speciation of Aquo Mo(VI) in Strong Acid

In strong acid solution (< pH 1) Mo(VI) at high dilution exists predominantly as the monomeric cation,[13] $(H_2O)_3MoO_2(OH)^+$. As the total Mo(VI) concentration is increased condensation leads to the formation of a series of dimeric cationic species. Equilibrium constants for the protonation and distribution of Mo(VI) among monomeric and dimeric forms in perchloric acid solutions have been evaluated from spectral measurements by Cruywagen and co-workers.[14] The significant equilibria are shown by equations 2.1-2.4.

$$Mo(OH)_6 + H^+ \rightleftharpoons Mo(OH)_5OH_2^+ \ (\equiv HMoO_3^+) \qquad (2.1)$$

$$2HMoO_3^+ \overset{k_d}{\rightleftharpoons} H_2Mo_2O_6^{2+} \qquad (2.2)$$

$$HMo_2O_6^+ + H^+ \rightleftharpoons H_2Mo_2O_6^{2+} \qquad (2.3)$$

$$H_2Mo_2O_6^{2+} + H^+ \rightleftharpoons H_3Mo_2O_6^{3+} \qquad (2.4)$$

We repeated their measurements in solutions of CF_3SO_3H and observed very similar spectra. We therefore adopted their approach to evaluate a conditional equilibrium constant for the monomer-dimer equilibrium in 2 M CF_3SO_3H:

$$K'_D = \frac{C_{Mo_2(VI)}}{C^2_{Mo(VI)}} \qquad (2.5)$$

where $C_{Mo(VI)}$ is the total concentration of monomeric Mo(VI) without regard to its state of protonation and $C_{Mo_2(VI)}$ is the corresponding

concentration of dimeric forms of Mo(VI). The value of K'_D at 25°C was 392 M^{-1}. (The value reported by Cruywagen et al. in 2M $HClO_4$ was 150 M^{-1}.)

Since we also found it desirable to examine the electrochemistry of Mo(VI) at 50°C in 2M CF_3SO_3H, K'_D was estimated from spectral measurements at this temperature. A value of 270 M^{-1} was obtained. A calculated distribution diagram for the sum of monomeric and dimeric forms of Mo(VI) at 25° and 50°C is given in Figure 2.4. Note that there is no sharp change in the concentrations of the monomeric and dimeric species at bulk concentrations near 0.1 to 0.2 mM where the sharp increase in adsorption of Mo(VI) occurs (Figure 2.3) The implication is that the species responsible for the adsorption is not one of the predominant forms in solution but is produced on the electrode surface, possibly as a result of condensation reactions among the predominant solution species that are present at concentrations of Mo(VI) greater than ca. 0.2 mM but exhibit only weak adsorption.

Pulse Polarography

Normal and reverse pulse polarography[15,16] were utilized to inspect the behavior of Mo(VI) at a dropping mercury electrode (Figure 2.5). At concentrations above 0.2 mM, normal pulse polarograms exhibited distorted shapes with current peaks preceding depressed limiting currents that signaled extensive adsorption of the reactant.[17] Reverse pulse polarograms were free of such distortions; however, the half-wave potential displayed a significant anodic shift. At concentrations below 0.1 mM normal pulse polarograms were also essentially undistorted (Figure 2.6). For a one-electron process the

Figure 2.4. Distribution of Mo(VI) between monomeric and dimeric forms as a function of the concentration of Mo(VI) at 25° (——) and 50°C (---) in 2 M CF_3SO_3H.

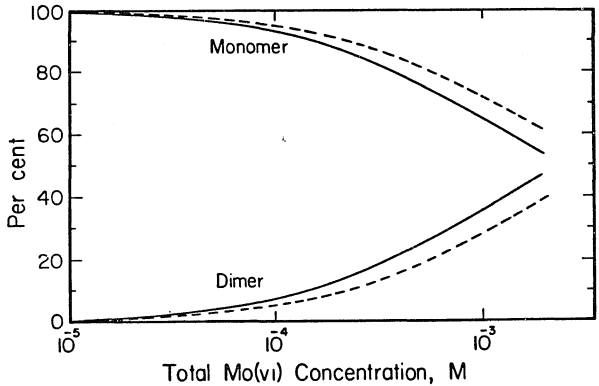
100
80
60
40
20
0
Per cent
Monomer
Dimer
10^{-5}
10^{-4}
10^{-3}
Total Mo(VI) Concentration, M

Figure 2.5. Normal and reverse pulse polarograms of 0.49 mM Mo(VI) in 2 M CF_3SO_3H. The drop time was 1 sec. The pulse widths were 1) 10.5, 2) 18.2 and 3) 36.3 msec.

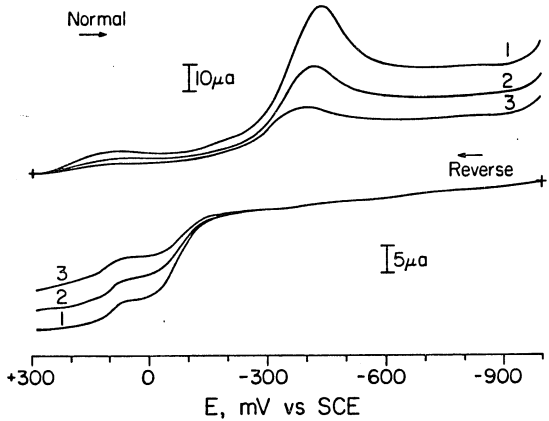
Normal
10μa
1
2
3
Reverse
5μa
3
2
1
+300
0
-300
-600
-900
E, mV vs SCE

Figure 2.6. Normal and reverse pulse polarograms of 0.05 mM Mo(VI) in 2 M CF_3SO_3H. Droptime: 1 sec.; pulse width: 10.5 msec. Inset: -E vs. log (i_L-i/i) for the normal pulse polarogram.

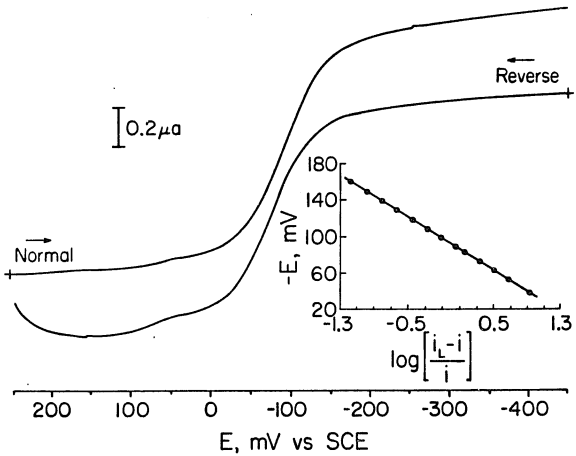
Reverse
0.2μa
Normal
180
140
100
60
20
-E, mV
-1.3
-0.5
0.5
1.3
log [i_L - i / i]
200
100
0
-100
-200
-300
-400
E, mV vs SCE

limiting reduction current in Figure 2.6, i_L, corresponds to a diffusion coefficient of 1.3×10^{-5} cm^2 s^{-1} for Mo(VI) at this high dilution where it exists predominantly as a monomeric ion (Figure 2.4). The plot of E vs. $\log(\frac{i_L - i}{i})$ shown in the inset in Figure 2.6 is linear with a slope of -57 mV pointing to a one-electron, nernstian electrode reaction. Reverse pulse polarograms recorded from an initial potential of 0.45 volt (where Mo(VI) is reduced to Mo(V) during the growth of each mercury drop before the potential is pulsed to more positive values) produced anodic limiting currents that were almost equal to the reduction currents obtained in the normal pulse polarograms of Mo(VI) so long as electrode drop times were restricted to 1 second or less. This is the behavior expected when a stable and re-oxidizable reduction product is produced at the electrode surface.[15,16] However, at longer drop times the ratio of anodic to cathodic currents decreased as expected when the product of the electrode process, Mo(V) in the present case, is unstable.

A plot of the normal pulse polarographic half-wave potentials for the reduction of Mo(VI) as a function of Hammet acidity (recorded with drop times short enough to avoid significant decomposition of the reduction product) is shown in Figure 2.7. The slope of 102 mV is reasonably close to the 118 mV value expected if the one-electron reduction reaction consumed two protons.

Cyclic Staircase Voltammetry

Conventional cyclic voltammetry with reactant solutions as dilute as those required to eliminate the complications from oligomerization and adsorption of Mo(VI) yields current responses that are dominated

Figure 2.7. Polarographic half-wave potential vs. Hammett acidity function, H_o, for reduction of monomeric Mo(VI) in CF_3SO_3H. The pK_a of the o-nitroaniline indicator used to evaluate H_o was taken as -0.3

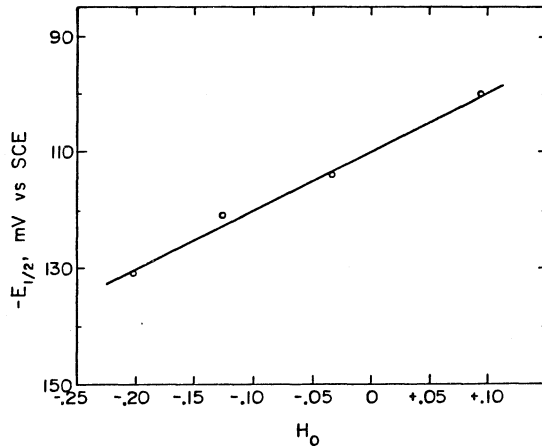
90
110
130
150
-E1/2, mV vs SCE
-.25
-.20
-.15
-.10
-.05
0
+.05
+.10
Ho

by the capacitive background current. Cyclic staircase voltammetry eliminates much of this capacitive charging current[10] and was therefore the preferred voltammetric method for these studies. Figure 2.8 shows a set of cyclic staircase voltammograms for several concentrations of Mo(VI). These voltammograms were recorded at 50°C because at this temperature higher concentrations of Mo(VI) could be utilized without encountering the severe adsorption that occurs near room temperature. A reversible couple is clearly evident near -0.1 volt and, in contrast with the behavior at room temperature or in more concentrated solutions, there is no dependence of the peak currents or wave shapes on the length of time the electrode is exposed to the solution before the voltammogram is recorded. The cathodic and anodic peak currents are equal and linearly dependent on the square root of the effective scan rate between 2 and 100 v s^{-1}. However, at scan rates below ca. 2 V s^{-1} the anodic peak current falls below its cathodic counterparts as the decomposition of Mo(V) begins to deplete its concentration at the electrode surface.

The separation of peak potentials in the cyclic staircase voltammograms is dependent on the effective scan rate and even at the lowest scan rates employed (1 V s^{-1}) it remained somewhat greater than the 80.6 mV value expected (at 50°C) when a 4.88 mV staircase step height is applied to a nernstian reaction (10 h). It is probable that both uncompensated resistance and slow electron transfer contributed to this behavior but we did not examine this feature in greater detail.

At concentrations of Mo(VI) greater than ca. 0.1 mM significant quantities of the dimeric ion are formed (Figure 2.4) and a wave which

Figure 2.8. Cyclic staircase voltammograms for Mo(VI) in 2 M CF_3SO_3H at 50°C. Initial potential: +0.25 V. Step time: 0.976 msec (effective scan rate = 5 V s^{-1}). Mo(VI) concentrations were A) 0.098; B) 0.24; C) 0.49 mM.

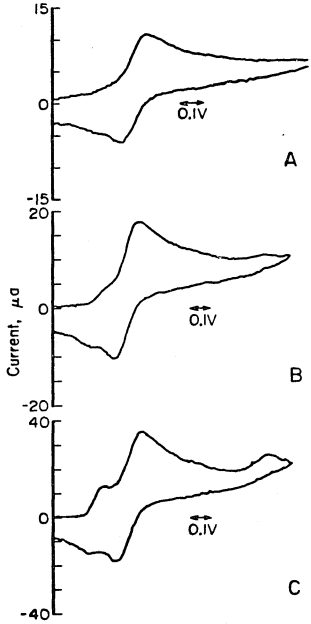
15
0
-15
0.1V
A
20
0
-20
0.1V
B
Current, μa
40
0
-40
0.1V
C

we believe to be due to the reduction of the dimer appears at more positive potentials in staircase voltammograms (Figure 2.8 B, C). By recording the voltammograms at sufficiently high effective sweep rates (>5 V s^{-1}) the monomer and dimer equilibrium were essentially "frozen" and the magnitudes of the two waves were compared with those calculated on the basis of the conditional equilibrium constant for the dimerization at 50°C in 2M CF_3SO_3H. Figure 2.9 shows a comparison of experimental staircase voltammograms with those obtained from a digital simulation of the staircase response for solutions containing a mixture of the monomeric and dimeric species. (The dimer was assumed to be reduced in a single, two-electron step and to have a diffusion coefficient 0.65 times as large as that of the monomer). The reasonable agreement between the observed and simulated voltammograms supports the assignment of the first wave to the reduction of dimeric Mo(VI).

At effective scan rates slower than 5 V s^{-1} the wave attributed to dimeric Mo(VI) increases at the expense of the monomeric Mo(VI) wave. The reported[18] value of k_f ($=1.71 \times 10^5$ M^{-1} s^{-1}) for reaction 2.2 measured by the temperature jump method in perchlorate media is consistent with this observation. Electrochemical measurement of this value was not possible due to the unknown diffusion coefficient of Mo_2(VI).

The reduction of the familiar, dimeric form of molybdenum (V), Mo_2(V),[19] is known to occur near -0.8 volt.[20] No wave corresponding to this process is evident in the staircase voltammograms for Mo(VI) when they are recorded at scan rates large enough to preserve equality

Figure 2.9. Comparison of experimental (left hand column) and simulated (right hand column) staircase voltammograms. The experimental voltammograms were taken from Figure 2.8 for potentials between +0.15 and -0.45 V.

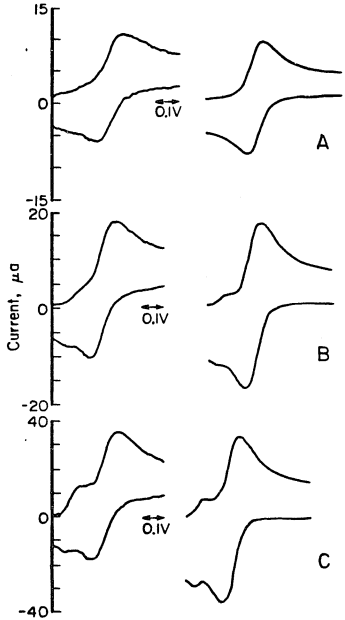
15
0
-15
0.1V
A
20
0
-20
Current, μa
0.1V
B
40
0
-40
0.1V
C

of the anodic and cathodic peak currents. However, at lower scan rates, where smaller anodic to cathodic peak current ratios result, a new wave begins to appear at the potential where $Mo_2(V)$ is reduced to $Mo_2(III)$ (Figure 2.8 B, C).[20] The clear implication is that the initial Mo(VI) reduction product undergoes a subsequent reaction leading to the formation of the stable molybdenum(V) dimer, $Mo_2(V)$.

Controlled Potential Electrolysis

Reduction of a 0.1 mM solution of Mo(VI) at a stirred mercury pool at -0.25 volt consumed one faraday per mole of Mo(VI). Voltammograms recorded during various stages of the electrolysis showed that a wave corresponding to the reduction of $Mo_2(V)$ to $Mo_2(III)$ developed as the original Mo(VI) reduction wave diminished. Thus, on the time scale of controlled potential electrolyses (20-40 minutes) the reduction of monomeric Mo(VI) produces $Mo_2(V)$.

Kinetics of the Disappearance of Mo(V)

Chronocoulometry provides a convenient procedure for evaluating the rates of chemical reactions entered into by the products of an electrode reaction.[21] The procedure involves the measurement of the ratio of faradaic charge consumed in the electrochemical production of an unstable species to the charge required for its subsequent electrochemical reconversion to starting material. This technique was applied to the Mo(VI)-Mo(V) system at a concentration of 0.1 mM and temperatures between 35° and 55°C to minimize adsorption. The data were analyzed by means of a working curve derived from a published digital simulation of the case that the chemical reaction is a second-order dimerization reaction[22] (see Appendix 2). The resulting dimerization

rate constant could be estimated only roughly because of complications from residual adsorption of Mo(VI), increasing concentration of dimeric Mo(VI), and the small signal-to-noise ratio. The values obtained at several temperatures and their estimated precision are shown in the Arrhenius plot in Figure 2.10. Extrapolation of the plot to 298°K leads to a rate constant of ca. $10^9\ M^{-1}\ s^{-1}$. The estimated activation enthalpy and entropy are 9 kcal/mole and -12 e.u., respectively.

Catalyzed Reduction of Perchlorate and Nitrate

If moderate amounts of perchloric or nitric acid are added to dilute solutions of Mo(VI) in 2 M CF_3SO_3H the resulting cyclic voltammograms (Figure 2.11) exhibit the features expected for a catalyzed regeneration of a reactant from its reduction product[23] (equation 2.6, 2.7).

$$Ox + ne \rightleftharpoons Red \qquad (2.6)$$

$$Red + Z \xrightarrow{k'} Ox + Y \qquad (2.7)$$

The current-voltage curve becomes flat rather than peaked, the anodic wave retraces the forward scan current, and the voltammograms are scan rate invariant under the conditions listed.

Since $Mo_2(V)$ does not react with either anion the catalytically active species seems likely to be the monomeric form of Mo(V). A quantitative determination of the stoichiometry of the catalytic reaction was not attempted with either anion due to the competing dimerization of monomeric Mo(V). However, chloride ion was observed to appear in long term reductions of Mo(VI) in the presence of perchlorate.

Figure 2.10. Arrhenius plot of chronocoulometrically determined rate constants governing the dimerization of Mo(V) monomer generated from 0.097 mM Mo(VI) in 2 M CF_3SO_3H.

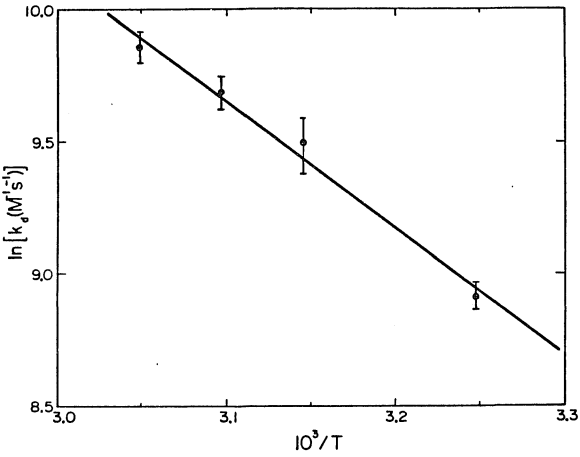
10.0
9.5
9.0
8.5
3.0
3.1
3.2
3.3
$10^3/T$
$\ln[k_e(M^{-1}s^{-1})]$

Figure 2.11. Effect of perchlorate and nitrate on the cyclic staircase voltammograms of 0.050 mM Mo(VI). Supporting electrolytes: 1) 1.9 M CF_3SO_3H + 0.1 M HNO_3, 2) 1.9 M CF_3SO_3H + 0.1 M $HClO_4$, 3) 2 M CF_3SO_3H. 50 mv s^{-1} scan rate.

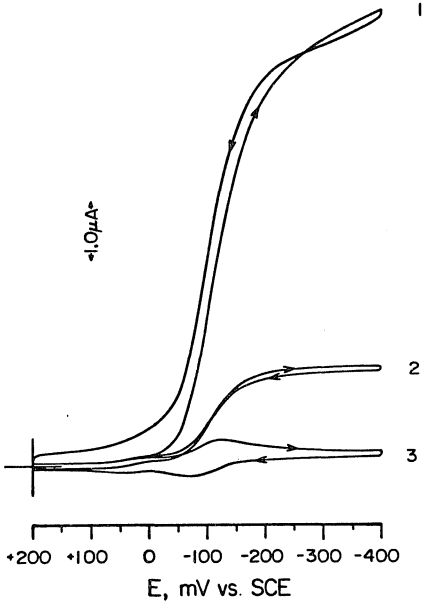
1
+1.0μA
2
3
+200 +100 0 -100 -200 -300 -400
E, mV vs. SCE

An extensive analysis of the theory of catalytic following reactions ($E_r C_i'$) has been reported by Saveant and Vianello.[24] In general, the experimental data and analysis assume that $C_Z \gg C_{ox}$. Under these conditions C_Z remains virtually constant and pseudo first-order conditions govern reaction 2.7. By defining the kinetic parameter $\lambda = k' C_Z t \left(= \frac{k' C_Z}{\gamma} \{\frac{RT}{nF}\}\right)$, where γ = scan rate, two limiting cases can be distinguished depending on the value of λ. In the region of small λ (< 0.04) voltammograms of substance Ox display normal diffusional behavior. When λ becomes greater than 1 the current attains a limiting value independent of scan rate which is given by equation 2.8.

$$(i_\infty)_c = nFAC_0 (D_{ox} K' C_Z)^{\frac{1}{2}} \tag{2.8}$$

Evaluation of k' can be accomplished using equation 2.8 or from the following equation which accounts for the stoichiometric factor (σ) in more complex catalytic schemes.[24]

$$\frac{(i_\infty)_c}{(i_p)_d} = \frac{\sqrt{\lambda}}{0.447} = \frac{1}{0.447} \cdot \sqrt{\frac{RT}{nF}} \cdot \sqrt{\frac{\sigma k' C_Z^0}{\gamma}} \tag{2.9}$$

Here $(i_p)_d$ is the current due to Ox in the absence of catalytic substrate Z at scan rate γ.

A somewhat consistent value of $(i_\infty)_c / C_Z^{0\,\frac{1}{2}}$ is obtained at several concentrations of C_Z^0 for both anions (Table 2.1). Assuming that the initial reaction of substrate with catalyst is rate determining, the apparent rate constants are $8.2 (\pm 1.2) \times 10^1\ M^{-1} s^{-1}$ for perchlorate and $1.2 (\pm 0.1) \times 10^3\ M^{-1} s^{-1}$ for nitrate.

Table 2.1

50 μM Mo(VI) $(i_p)_d = 0.36$ μa

I = 2.0 adjusted with HTFMS

50 mv/s

$HClO_4$ = Z

C_Z, M	$(i_\infty)_c/C_Z^{o\frac{1}{2}}$ (μA/M)	$(i_\infty)_c/(i_p)_d$	$\sigma k'$ (M^{-1} s^{-1})
0.05	5.6	3.5	96.
0.10	4.7	4.1	65.
0.20	5.0	6.2	75.
0.5	5.5	10.8	91.
		avg. = 82 ± 12 M^{-1} s^{-1}	

HNO_3 = Z

C_Z^o, M	$(i_\infty)_c/C_Z^{o\frac{1}{2}}$ (μA/M)	$(i_\infty)_c/(i_p)_d$	$\sigma k'$ (M^{-1} s^{-1})
0.05	4.6	13	1.3×10^3
0.10	6.4	18	1.2×10^3
0.20	9.2	26	1.3×10^3
0.50	13.8	38	1.1×10^3
		avg. = $1.2 \pm 0.1 \times 10^3$ M^{-1} s^{-1}	

Discussion

The important monomeric forms of Mo(VI) present in strongly acidic solutions were termed molybdic acid and protonated molybdic acid by Cruywagen et al.[14] who wrote the formulae $Mo(OH)_6$ and $Mo(OH)_5OH_2^+$, respectively. We prefer to depict these two species in equation 2.1 as trioxo and cis-dioxo derivatives as shown below:

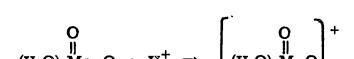

(2.10)

for which Cruywagen et al.[14] report an equilibrium constant of 11.4 M^{-1}. Thus, in 2M CF_3SO_3H, over 95% of the monomeric Mo(VI) is present as 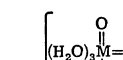 . As shown in Figure 2.4, dimer formation does not exceed several percent with concentrations of Mo(VI) of 0.1 mM or less so that under these conditions the observed electrochemistry should be that of the dioxo cation 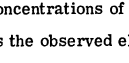 .

The pattern of electrochemical responses exhibited by dilute solutions of Mo(VI) is consistent with the following pair of reactions governing the course of the reduction:

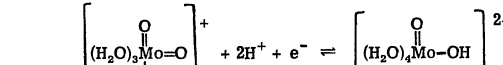

(2.11)

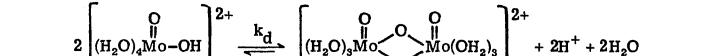

(2.12)

Reaction 2.11 takes account of the pH dependence of the half-wave potential for the reduction of Mo(VI) (Figure 2.7) and reaction 2.12 is based on a plausible structure that has been proposed for the stable dimer of Mo(V).[18,25] Direct evidence for the reverse of reaction 2.12 is sparse: Murman has measured the kinetics of the exchange with the solvent of labeled bridging oxo groups in the Mo(V) dimer[26] but the mechanism of this process need not include the reverse of reaction 2.12. Epr signals for several monomeric complexes of Mo(V) have been reported,[27] but such experiments have always involved the presence of added ligands that form very stable complexes with Mo(V).

The kinetics of dimerization of a monomeric Mo(V) catechol complex were reported recently[28] and a mechanism proposed that shares several of the features of reactions 2.11 and 2.12. However, large differences in pH and solution compositions prevent a more detailed comparison.

Since the Mo(V) monomer, but not the dimer,[20] exhibits an anodic wave at -0.2 volt (Figure 2.8) we sought to detect any monomer in equilibrium with the dimer by means of anodic normal pulse polarography with a 10 mM solution of $Mo_2(V)$ prepared by exhaustive electrolytic reduction of Mo(VI) in 2M CF_3SO_3H. No anodic response above background levels was detected in this experiment. We estimate the maximum concentration of monomer that could have gone undetected as 6×10^{-6} M which places a lower limit of ca. 10^9 M (25° C) on the

equilibrium constant for reaction 2.12 (assuming that the proton dependence is correct as shown).

The value estimated for the rate constant governing the dimerization of Mo(V), $k_d \sim 10^3\ M^{-1}\ s^{-1}$ (25° C), is qualitatively consistent with the behavior observed in the normal and reverse pulse polarographic experiments with 5×10^{-5} M solutions of Mo(VI) (Figures 2.5). For example, the ratio of anodic to cathodic limiting current decreased from unity to 0.71 as the drop time was increased from 1 to 5 seconds compared with a calculated value of 0.79 assuming simple, second-order irreversible loss of the Mo(V) throughout the 5 second drop life.

Although reoxidation of the monomeric form of Mo(V) to Mo(VI) appears to proceed readily at the mercury electrode, no further reduction of the monomer was observed before decomposition of the solvent commences at ca. -1.0 volt. This resistance of monomeric Mo(V) towards electro-reduction to Mo(IV) matches the behavior of the monomeric Mo(III) ion, $Mo(OH_2)_6^{3+}$, which is not oxidized to Mo(IV) at mercury electrodes.[20] The apparent barrier to the generation of a monomeric form of aquo Mo(IV) is probably associated with the strong preference of this oxidation state to form multi-nuclear ions: The stable form of aquo Mo(IV) has been argued to contain one,[29] two[30] and three[18,31] molybdenum centers but the correct structure appears to be the trimeric ion, $Mo_3O_4^{4+}$.[31,32] The structural differences separating the monomeric Mo(III) ion, $Mo(OH_2)_6^{3+}$, and the structure proposed for monomeric Mo(V) in equation 2.11 do not appear to be large but the difficulty in passing through the evidently unstable monomeric Mo(IV) state to reach $Mo(OH_2)_6^{3+}$ is presumably responsible for

the absence of a two-electron reduction of the Mo(V) monomer. In an earlier report[20] on the pulse polarography of monomeric $Mo(OH_2)_6^{3+}$ (with the initial electrode potential at +0.15 volt) a prominent reduction wave was observed near -0.1 volt that was tentatively ascribed to the reduction of monomeric Mo(V) generated at the electrode surface by oxidation of $Mo(OH_2)_6^{3+}$. The present results indicate that monomeric Mo(V) is not reducible in the accessible potential range but that the reduction of monomeric Mo(VI) proceeds near -0.1 volt. For this reason assigning the wave at -0.1 volt in the pulse polarography of $Mo(OH_2)_6^{3+}$ to the reduction of Mo(VI) monomer generated by the (very slow)[20] oxidation of $Mo(OH_2)_6^{3+}$ at +0.15 volt seems plausible.

The general aspects of atom transfer reactions with regard to the reduction of perchlorate and nitrate ions by transition metal ions have been addressed by Taube.[33] Presently, there is no well defined correlation between ΔG and reactivity or a good understanding of why $1e^-$ reductants are as reactive or more so than $2e^-$ reductants. The reactivity of monomeric Mo(V) towards perchlorate and nitrate ions is thought to be related to its ability to stabilize O^{2-} and form an "yl" product, namely the Mo(VI) cation, $\left[(H_2O)_3\overset{O}{\overset{\|}{Mo}}\overset{}{=}O\right]^{+}$ (OH).

Monomeric Mo(V) is an extremely reactive $1e^-$ reductant possessing a rate constant ca. 10^6 larger than the more well characterized $1e^-$ reductant, Ti(III).[34]

The reduction of perchlorate and nitrate is not limited to the monomeric Mo(V) ion shown in equation 2.11. Deaerated solutions of

trimeric Mo(IV) are only stable for periods of ca. one day in solutions containing perchlorate.[29] In addition, the Bowen-Taube ion, $Mo(H_2O)_6^{3+}$, reduces nitrate with a rate constant of 2.9×10^{-2} l. M^{-1} s^{-1} according to the following stoichiometry.[35]

$$2Mo(H_2O)_6^{3+} + 2NO_3^- \rightarrow Mo_2O_4(H_2O)_8^{2+} + 2NO_2^- + 4H^+ + 4H_2O \quad (2.13)$$

It is interesting to note that the Mo(V) monomer produced by acidification (> 6 N HCl) of $Mo_2O_4(H_2O)_8^{2+}$ is not reactive towards perchlorate.[36] Apparently the $[(H_2O)_4\overset{O}{\overset{\|}{M}}o\text{-}OH]^{2+}$ unit is required for significant reactivity.

Adsorption of Mo(VI)

The sudden onset of extensive adsorption of Mo(VI) at bulk concentrations greater than ca. 0.2 mM (Figure 2.3) is not typical of simple ionic adsorption at mercury.[37] It is more reminiscent of adsorption that appears to result in the formation of new phases containing multilayers of the adsorbate on the surface.[38] The behavior of Mo(VI) differs from most previous examples[39] in that no complex-forming ligands are required to induce the adsorption. The well-known tendency for Mo(VI) to condense spontaneously into oligomeric ions as its concentration is increased[40] seems likely to underlie the adsorption. Specifically adsorbed Mo_2(VI) may be an initiator for this surface condensation process. At concentrations above 1 mM or so the electrode surface appears to become covered with a film of condensed polymolybdate of unknown composition that interferes with the reduction of Mo(VI) from the bulk of the solution leading to the distorted and

depressed polarograms and voltammograms that are so familiar in the electrochemistry of Mo(VI).[2-6]

Conclusions

Highly dilute acidic solutions of Mo(VI) in which monomeric ions predominate exhibit much simpler electrochemistry than results with less dilute solutions. A reversible redox couple consisting of monomeric Mo(VI) and Mo(V) ions can be observed in such solutions. The aquo Mo(V) ion undergoes spontaneous dimerization to form the stable Mo_2(V) ion which is not oxidizable at mercury electrodes. The monomeric form of Mo(V) is not further reduced in the accessible range of potentials probably because of the intrinsic instability of the monomeric Mo(IV). This monomeric Mo(V) species is catalytically active towards reduction of perchlorate and nitrate.

References and Notes

1. A slightly different version of this chapter has appeared in print: Paffett, M. T. and Anson, F. C., Inorg. Chem., 1981, 20, 3967.
2. Haight, G., Inorg. Nucl. Chem., 1962, 24, 673.
3. Lamache, M. and Souchay, P., J. Chim. Phys., 1973, 2, 384.
4. Lamache, M.; Cadiot, J. and Souchay, P., J. Chim. Phys., 1968, 65, 1921.
5. Hull, M., Jr., Electroanal. Chem., 1974, 51, 57.
6. Wittick, J. and Rechnitz, G., Anal. Chem., 1965, 37, 816.
7. Belcher, R. and Nutten, A. J., "Quantitative Inorganic Analysis", 2nd ed., Butterworths, London, 1960, p. 133.
8. Abel, R.; Christie, J.; Jackson, L.; Osteryoung, J. and Osteryoung, R., Chem. Instrum. 1976, 123.
9. Lauer, G.; Abel, R. and Anson, F., Anal. Chem., 1967, 39, 765.
10. (a) Barker, G. C., Adv. Polarography, 1960, 1, 144; (b) Christie, J. H. and Lingane, P. J., J. Electroanal. Chem. 1965, 10, 176; (c) Mann, C. K., Anal. Chem., 1961, 33, 1484; (d) Mann, C. K., Anal. Chem., 1965, 37, 326; (e) Zipper, J. J. and Perone, S. P., Anal. Chem., 1973, 45, 452; (f) Ferrier, D. R. and Schroeder, R. R., J. Electroanal. Chem., 1973, 45, 353; (g) Ryan, M. D., J. Electroanal. Chem., 1977, 79, 105; (h) Miaw, H.-L. and Perone, S. P., Anal. Chem. 1978, 50, 1989.
11. Nicholson, R. and Olmstead, M., in "Electrochemistry: Calculations, Simulation and Instrumentation", Mattson, J.; Mark, H. and MacDonald, H. Eds., Marcel Dekker, New York, 1972, p. 119.

(12) Bard, A. J. and Faulkner, L. R., "Electrochemical Methods", John Wiley and Sons, New York, N.Y., 1980, p. 199.

(13) Chojnacka, J., Roczniki Chem., 1965, 89, 161.

(14) Cruywagen, J., Heyns, J. and Rohwer, E., J. Inorg. Nucl. Chem., 1978, 40, 53.

(15) Oldham, K. and Parry, E., Anal. Chem., 1970, 42, 229.

(16) Osteryoung, J. and Kirowa-Eisner, E., Anal. Chem., 1980, 52, 62.

(17) Flanagan, J. B., Takahashi, K. and Anson, F. C., J. Electroanal. Chem., 1977, 85, 257.

(18) Ojo, J. F.; Taylor, R. S. and Sykes, A. G., J. Chem. Soc. Dalton, 1975, 500.

(19) Cotton, F. A. and Wilkinson, G., "Advanced Inorganic Chemistry", John Wiley and Sons, New York, N.Y., 4th ed., p. 868.

(20) Chalilpoyil, P. and Anson, F. C., Inorg. Chem., 1978, 17, 2418.

(21) Christie, J. H., J. Electroanal. Chem., 1967, 13, 79; Ridgeway, T. H., Reilley, C. W. and Van Duyne, R. P., J. Electroanal. Chem., 1976, 67, 1.

(22) Childs, W.; Maloy, J.; Keszthelyi, C. and Bard, A. J., J. Electrochem. Soc., 1971, 118, 872.

(23) Ref. 12, p. 455.

(24) Saveant, J. M. and Vianello, E., Electrochim. Acta, 1965, 10, 905.

(25) Ardon, M. and Pernick, A., J. Less Common Met., 1977, 54, 233.

26. Murman, K., Inorg. Chem., 1980, 19, 1765.

27. Sacconi, L. and Cini, R., J. Am. Chem. Soc., 1954, 76, 4239; Spence, J. T. and Heydanek, M., Inorg. Chem. 1967, 6, 1489; Huang, T. J. and Haight, Jr., G. P., J. Am. Chem. Soc., 1970, 92, 2336; ibid., 1971, 93, 611; Imamura, T.; Haight, Jr., G. P., and Belford, R. L., Inorg. Chem., 1976, 15, 1047; Haight, G. P.; Woltermann, G.; Imamura, T. and Hummel, P., J. Less Common Met., 1977, 54, 121.

28. Charney, L. M. and Schultz, F. A., Inorg. Chem., 1980, 19, 1527.

29. Ojo, J. F.; Sasaki, Y.; Taylor, R. and Sykes, A. G., Inorg. Chem., 1976, 15, 1006.

30. Ardon, M.; Bino, A. and Yahav, G., J. Am. Chem. Soc. 1976, 98, 2338; Cramer, S. P.; Gray, H. G.; Dori, Z. and Bino, A., J. Am. Chem. Soc., 1979, 101, 2770.

31. Cramer, S. P.; Eidem, P. K.; Paffett, M. T.; Winkler, J. R.; Dori, Z. and Gray, H. B., J. Am. Chem. Soc., 1983, 105, 799.

32. Murmann, R. K. and Shelton, M. E., J. Am. Chem. Soc., 1980, 102, 3984.

33. Taube, H., in "Mechanistic Aspects of Inorganic Reactions", Rorabacher and Endicott Eds., American Chem. Soc., 1982, Ch. 7.

34. Cope, V. W.; Miller, R. G. and Fraser, R. T. M., J. Chem. Soc. A, 1967, 301.

35. Ketchum, P. A.; Taylor, R. C. and Young, D. C., Nature, 1976, 259, 202.

36. Haight, G. P., J. Inorg. Nucl. Chem., 1962, 24, 663.

37. Delahay, P., "Double Layer and Electrode Kinetics", Wiley Interscience, New York, N.Y., 1965, Ch. 4.

38. Elliott, C. M. and Murray, R. W., J. Am. Chem. Soc., 1974, 96, 3321; Parkinson, B. A. and Anson, F. C., Anal. Chem., 1978, 50, 1886.

39. Anson, F. C., Accts. Chem. Res. 1975, 8, 400.

40. Reference 18, p. 852 ff.

CHAPTER 3

Observations on the Electrochemistry of the Dimeric Mo(V) - Dimeric Mo(III) Redox Couple

Introduction

The efficient reduction of small molecules such as O_2, N_2, and C_2H_2 requires chemical moieties capable of multiple electron transfers. In attempts to mimic the catalytic reactions of metalloenzymes dimeric molecules capable of multiple electron transfer have attracted considerable attention.[1] An example of this is the use of the $Mo_2(V)/Mo_2(III)$ redox couple in the presence of complexing ligands as a catalyst for acetylene reduction.[2-4] Although these systems possess no reactivity toward nitrogen it is noteworthy that biological nitrogen-fixing systems also reduce acetylene. With regard to small molecule reductions the electrochemical behavior of the $Mo_2(V)/Mo_2(III)$ redox couple is of interest.

Reduction of the dimeric Mo(V) aquo ion leads directly to a dimeric Mo(III) product, without passing through a stable Mo(IV) state.[5] This multi-electron, multi-proton redox reaction is noted for its highly irreversible character. Specific factors which contribute to the sluggish electrode kinetics will be addressed by an electrochemical study of the aquo ion and oxalate derivative.

Experimental

Materials

Solvent and electrolyte preparation are mentioned in Chapter 2. Reagent grade sodium molybdate was used as received. Solutions of $Mo_2O_4^{2+}$ were prepared by electrochemical reduction (Chapter 2) or by reduction with hydrazine sulfate followed by ion exchange purification with Bio-Rad AG 50W-X2 cation exchange resin. Solutions were

deoxygenated by sparging with argon gas passed through solutions of either chromium(II) or vanadium(II). Buffered oxalate solutions were prepared from oxalic acid and potassium oxalate. The extinction coefficient of $Mo_2O_4^{2+}$ was determined to be $3210 \pm 100\ M^{-1}cm^{-1}$ at 296 nm in 2M trifluoromethanesulfonic acid by oxidation with standardized ceric ion solution. This value compared well with the value ($3370\ M^{-1}\ cm^{-1}$) reported[6] in 1M perchloric acid. Concentrations were evaluated spectrally using $\epsilon = 3210\ M^{-1}cm^{-1}$.
$NH_4[Mo_2O_4(C_2O_4)_2(H_2O)_2]$ was prepared by literature methods[7] or was generously supplied by Jay Winkler.

Instrumentation

Electrochemical and absorption spectroscopy instruments are described in Chapter 2.

Results

Mo_2(V) aquo ion

The general features of the chemically reversible $Mo_2(V)/Mo_2(III)$ aquo ion redox couple were recently described by Chalilpoyil and Anson.[5] Among the observations reported were an overall four electron reduction to Mo_2(III), very irreversible electron transfer properties, an apparent proton dependence in the reduction potential, and a slow chemical step preceding the four electron reoxidation of Mo_2(III) to Mo_2(V). These experimental observations will be examined in detail using several electrochemical techniques.

Cyclic voltammograms of the Mo_2(V) aquo ion at two different acidities are shown in Figure 3.1. The wave shapes are very

Figure 3.1. Cyclic voltammograms of A) 1.1 mM $Mo_2(V)$ in 0.2 M HTFMS + 1.8 M LiTFMS and B) 0.56 mM $Mo_2(V)$ in 2.0 M HTFMS at scan rates of 1) 200, 2) 100, 3) 50, 4) 20 and 5) 10 mV s^{-1}.

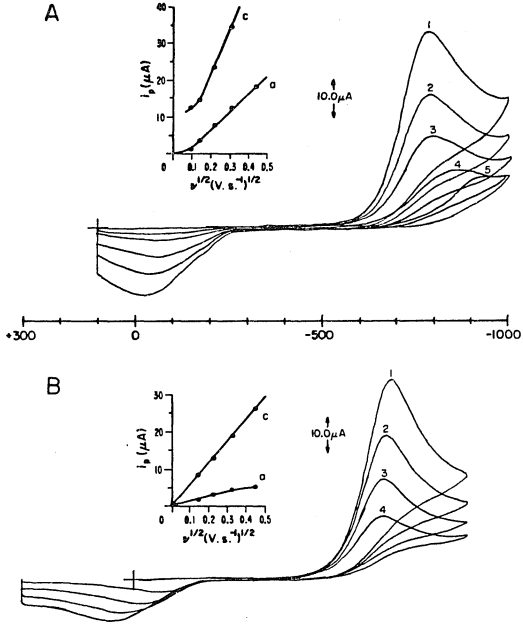
A
c
a
i_p (μA)
$v^{1/2}$(V. s.$^{-1}$)$^{1/2}$
10.0μA
1
2
3
4
5
+300
0
-500
-1000
B
c
a
i_p (μA)
$v^{1/2}$(V. s.$^{-1}$)$^{1/2}$
10.0μA
1
2
3
4

asymmetric with a large potential separation between the cathodic and anodic peaks and an anodic/cathodic peak current ratio of much less than unity. At scan rates between 0.02 and 0.2 V s^{-1} the reduction process is diffusion controlled as determined from plots of i_{pc} versus (scan rate)$^{\frac{1}{2}}$ (inset Figure 3.1). At lowered acidity the reduction peak shifts to more negative potentials and the anodic/cathodic peak current ratio increases. Also at lower acidity the slow scan voltammograms (ca. 0.01-0.02 V s^{-1}) of Figure 3.1A display an unusual negative shift of the cathodic peak potential and a cathodic current increase above that expected for a diffusion controlled reaction. Presently, there is no explanation for this observation.

Voltammograms at faster scan rates were recorded using the cyclic staircase technique. The inherent advantages of this technique were discussed in Chapter 2. Most of the qualitative features observed in the cyclic voltammograms are seen in the staircase voltammograms (Figure 3.2). These features include very asymmetric wave shapes, a negative shift in peak potentials with effective scan rate, diffusion controlled reduction peaks as judged by linear i_{pc} versus (step time)$^{-\frac{1}{2}}$ behavior (inset Figure 3.2), and anodic/cathodic peak current ratios that are less than unity. The decrease in anodic current is more pronounced at the faster scan rates. In Figure 3.2B the anodic current is scan rate invariant for effective scan rates above 0.5 V s^{-1} In less acidic solution (Figure 3.2A) the voltammograms show a slight increase in anodic current with increasing effective scan rate; however, at sufficiently fast effective scan rates (>5.0 V s^{-1}) the anodic current is independent of scan rate. Reoxidation of Mo_2(III) to Mo_2(V)

Figure 3.2. Cyclic staircase voltammograms of A) 1.0 mM $Mo_2(V)$ in 0.2 M HTFMS + 1.8 M LiTFMS and B) 1.1 mM $Mo_2(V)$ in 2 M HTFMS at effective scan rates of 1) 5.0, 2) 2.0, 3) 1.0, and 4) 0.5 V s^{-1}.

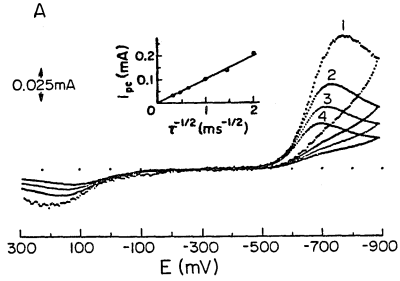
A
0.025mA
i_{pc} (mA)
0.2
0.1
0
1
2
$\tau^{-1/2}$ (ms$^{-1/2}$)
1
2
3
4
300
100
-100
-300
-500
-700
-900
E (mV)

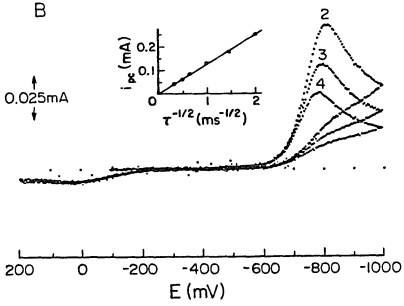
B
0.025mA
i_{pc} (mA)
0.2
0.1
0
1
2
$\tau^{-1/2}$ (ms$^{-1/2}$)
2
3
4
200
0
-200
-400
-600
-800
-1000
E (mV)

is preceded by a chemical step displaying an inverse proton dependence.

The normal and reverse pulse polarograms clearly demonstrate the highly irreversible nature of the $Mo_2(V)/Mo_2(III)$ redox couple (Figure 3.3). A general description of the following terminology and theory of pulse polarographic current-potential curves is given in Appendix 3. The reverse pulse polarograms are split into two well separated components, as expected for an electrode reaction with very slow electron transfer properties.[8] In addition, the total reverse pulse limiting current ($i^{\ell}_{RP1} + i^{\ell}_{RP2}$) in 2 M HTFMS is substantially less than the normal pulse limiting current (i^{ℓ}_{NP}) for all pulse widths. In less acidic solutions (0.2 M HTMS: Figure 3.3B) the ratio of total reverse pulse limiting current ($i^{\ell}_{RP1} + i^{\ell}_{RP2}$) to normal pulse limiting current (i^{ℓ}_{NP}) is approximately unity at long pulse widths. Table 3.1 lists the values of $i^{\ell}_{RP1}/i^{\ell}_{NP}$ for different acidities and pulse widths. Reasonable agreement is found with theory for irreversible electron transfers at all pulse width variations. In Table 3.2 the ratios $(i^{\ell}_{RP1} + i^{\ell}_{RP2})/i^{\ell}_{NP}$ are given for the same acidity range and pulse width variation. As seen from the data decreasing the time parameter (pulse width) results in a progressively decreasing value of $(i^{\ell}_{RP1} + i^{\ell}_{RP2})/i^{\ell}_{NP}$. This is consistent with a chemical step preceding the reoxidation of $Mo_2(III)$ to $Mo_2(V)$. Again, the preceding chemical reaction displays an inverse proton dependence such that at the lowest acidities (0.048M HTFMS) the reverse and normal pulse limiting currents were essentially equal at all pulse widths. It was not possible to work in solutions less acidic than pH ca. 1.5 because the reduction wave shifts into the background

Figure 3.3. Normal (N) and reverse (R) pulse polarograms of 1.1 mM Mo_2(V) in A) 2.0 M HTFMS and in B) 0.2 M HTFMS + 1.8 M LiTFMS at a pulse width of 18.2 ms and a 1 s drop time.

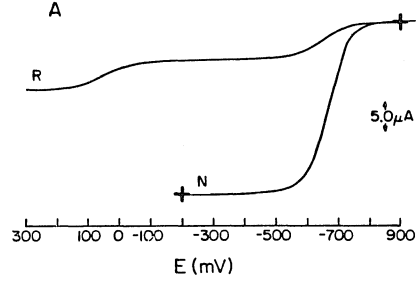
A
R
5.0μA
N
300
100
0
-100
-300
-500
-700
900
E (mV)

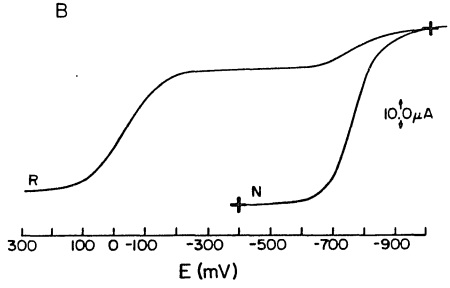
B
10.0μA
R
N
300
100
0
-100
-300
-500
-700
-900
E (mV)

Table 3.1. Ratio of Reverse Pulse Current 1 to Normal Pulse Current

Pulse width τ_m (ms)	Theoretical value[a] $i^{\ell}_{RP1}/i^{\ell}_{NP}$	Experimental Values $i^{\ell}_{RP1}/i^{\ell}_{NP}$				
		$[H^+]^b = 2.0$	1.0	0.5	0.2	0.048
95.5	0.472	0.50	0.52	0.55	0.53	0.55
54.9	0.358	0.39	0.39	0.42	0.41	0.42
18.2	0.206	0.23	0.23	0.24	0.24	0.29
10.5	0.156	0.18	0.18	0.19	0.18	0.22
5.05	0.109	0.13	0.13	0.13	0.13	0.16

a. Reference 9.

b. Ionic strength adjusted to 2.0 with LiTFMS.

Table 3.2. Ratio of Total Reverse Pulse Current to Normal Pulse Current

Pulse width		Experimental Values			
τ_m		$(i^{\ell}_{RP1} + i^{\ell}_{RP2})/i_{NP}$			
(ms)	$[H^+]^a = 2.0$	1.0	0.5	0.2	0.048
95.5	0.75	0.93	1.12	1.07	1.09
54.9	0.62	0.80	1.00	1.03	1.06
18.2	0.41	0.62	0.80	0.98	1.09
10.5	0.28	0.51	0.72	0.87	0.99
5.05	0.24	0.42	0.57	0.79	0.99

a. Ionic strength adjusted to 2.0 with LiTFMS.

discharge current due to hydrogen production.

The normal pulse current-potential curves were analyzed in the fashion prescribed by Oldham and Parry[9] by plotting $\log[\frac{x^2(1.75+x^2)}{(1-x)}]$ versus -E, where x is i/i_d. The slope of the resulting line is equal to $\frac{2\alpha n_a}{59}$ (mV^{-1}), where α is the transfer coefficient, and n_a is the number of electrons involved in the rate determining step. Figure 3.4 displays such normal pulse polarographic log plots for the $Mo_2(V)$ aquo ion. The product αn_a is determined to be ca. 0.73 over the acidity range 2.0 to 0.048 M HTFMS in the absence of a double layer correction.[10] The shift in half wave potential with H_0 is 106 mV per H_0 unit. The reaction order with respect to protons can be determined from a plot of log x versus H_0, under conditions of electrochemical irreversibility ($x \leq 0.12$). The slope of the line in such a plot is 1.4 (Figure 3.5). The significance of this value is explained in the discussion section. The normal pulse limiting currents are equivalent to an overall four electron reduction with a diffusion coefficient of 3.2×10^{-6} $cm^2 s^{-1}$ in 2 M HTFMS. The value of k_s could not be determined since the standard potential for the $Mo_2(V)/Mo_2(III)$ redox couple is not presently known.

The chemical reaction preceding reoxidation of the $Mo_2(III)$ aquo ion was also qualitatively examined using double potential step chronocoulometry. As described in Appendix 2 a key experimental observable relevant to the homogeneous solution chemistry is the ratio of charge at the end of the reverse step to that at the end of the forward step (Q'_B/Q_F; assuming appropriate correction for double layer charging). For the $Mo_2(V)/Mo_2(III)$ redox couple the initial potential

Figure 3.4. Normal pulse polarographic log plots for $Mo_2(V)$ reduction in (•) 2.0 M, (+) 1.0 M, (□) 0.5 M, (▲) 0.2 M and (○) 0.048 M HTFMS. The pulse width was 54.9 ms and the drop time was 1 s.

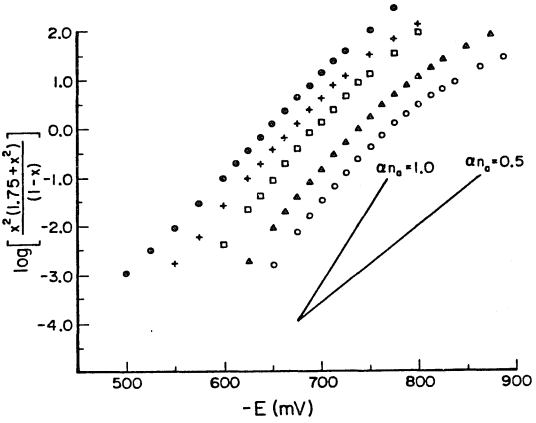
2.0
1.0
0.0
-1.0
-2.0
-3.0
-4.0
500
600
700
800
900
-E (mV)
$\log\left[\frac{x^2(1.75+x^2)}{(1-x)}\right]$
$\alpha n_a = 1.0$
$\alpha n_a = 0.5$

Figure 3.5. Proton reaction order log plot for the $Mo_2(V)$ aquo ion reduction.

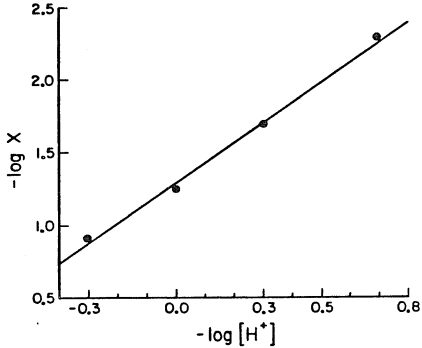
2.5
2.0
1.5
1.0
0.5
-log X
-0.3
0.0
0.3
0.5
0.8
-log [H+]

was stepped to a value sufficiently negative to insure diffusion controlled reduction of $Mo_2(V)$. The reverse potential step was ca. 200 mV positive of the apparent oxidation peak of $Mo_2(III)$. So that, in the absence of the homogeneous preceding chemical reaction, the reoxidation should have proceeded at the diffusion controlled rate. However, the observed ratio of Q'_B/Q_F is substantially less than that predicted from theory for diffusion controlled reduction and reoxidation (0.5858). Table 3.3 lists the experimental values of Q'_B/Q_F for the $Mo_2(V)/Mo_2(III)$ couple at various switching times (τ) and acidities. Noteworthy are the increasing values of Q'_B/Q_F at all acidities as τ increases. The inverse proton dependence in the chemical reaction preceding reoxidation is also manifest from the Q'_B/Q_F values. The charge ratios displayed no dependence on total concentration of $Mo_2(V)$.

Controlled potential electrolysis of the $Mo_2(V)$ aquo ion has been reported[5] to consume four electrons per equivalent of dimer in producing the $Mo_2(III)$ aquo ion. Fully reduced solutions possess an absorption spectrum identical to that of the $Mo_2(III)$ aquo ion.[11] Reoxidation of the $Mo_2(III)$ aquo ion has been reported to be sluggish, evidently due to an intervening chemical step. Attempts to duplicate the coulometric reduction of $Mo_2(V)$ produced variable results. Although the reduced solutions produced the correct absorption spectrum for $Mo_2(III)$ the number of equivalents required to reach background current levels exceeded four by several fold. In spite of this difficulty, it was possible to reduce the $Mo_2(V)$ aquo ion quantitatively to $Mo_2(III)$ and subsequently to reoxidize the $Mo_2(III)$ aquo ion back to $Mo_2(V)$.

Table 3.3. Experimental values of Q'_B/Q_F for Double Potential[a] Step Chronocoulometry of $Mo_2(V)/Mo_2(III)$.

					τ(s)				
$[H^+]^b$	0.5	0.25	0.20	0.15	0.10	0.075	0.05	0.025	0.01
2.0		0.221	0.195		0.160		0.130	0.10	0.08
1.0		0.348	0.321	0.320	0.295	0.272	0.252	0.224	
0.5	0.464		0.422		0.385		0.347	0.296	0.280
0.2		0.490	0.482	0.471	0.471	0.445	0.428	0.394	
0.048				0.479		0.489	0.471	0.484	0.453

a. Potential steps explained in text.

b. Ionic strength adjusted to 2.0 with LiTFMS.

$Mo_2O_4(C_2O_4)_2(H_2O)_2^{2-}$

The reduction of this $Mo_2(V)$ derivative was studied in the pH range 2.5 to 5.0 in buffered oxalate solutions. The electrochemical responses exhibited by the oxalate derivative will be compared with those reported by Schultz et al.[12,13] for the cysteine and edta derivatives. In addition, the information gained in this less acidic region complements the electrochemistry of the uncomplexed $Mo_2(V)$ aquo ion described in the previous section.

Cyclic voltammograms of $Mo_2O_4(C_2O_4)_2(H_2O)_2^{2-}$ in oxalate media are characterized by a highly irreversible reduction (Figure 3.6). The reduction peak is diffusion controlled as judged from the linear dependence of peak current on $(\text{scan rate})^{\frac{1}{2}}$ (see inset in Figure 3.6 A,B). The reduction peak potential shifts to more positive potentials with increasing acidity suggesting coupled proton-electron transfer in the reduction process. The anodic current is very dependent on scan rate and pH of the medium. At sufficiently fast scan rates (ca. 1 V s^{-1}) one anodic wave is seen ca. 600 mV positive of the reduction peak. As the scan rate decreases the relative height of the anodic wave decreases and other waves at more positive potentials appear. The behavior is more complex in the less acidic solution (pH = 4.69), with as many as three waves appearing.

In the more acidic solution (pH $\leq$ 3.1) two anodic waves are obtained at 0.02 V s^{-1}, with the predominant one centered at ca. -400 mV. Throughout the pH range studied the anodic currents never attained the magnitude of the original cathodic current.

Figure 3.6. Cyclic voltammograms of 0.9 mM $Mo_2O_4(C_2O_4)_2(H_2O)_2^{2-}$ in A) pH 4.69 and B) pH 3.07 oxalate media at scan rates 1) 200, 2) 100, 3) 50, 4) 20, and 5) 10 mV s^{-1}. Ionic strength adjusted to 0.5 with KCl.

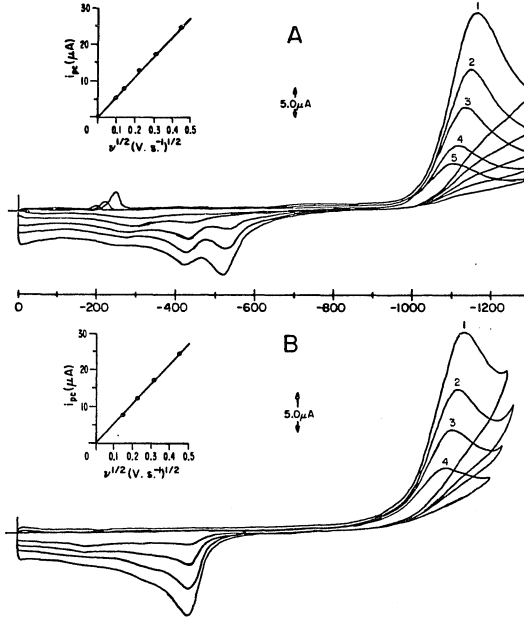
A
B
5.0μA
5.0μA
1
2
3
4
5
0
-200
-400
-600
-800
-1000
-1200
i_{pc} (μA)
$\nu^{1/2}$ (V. s^{-1})$^{1/2}$

Controlled potential electrolysis of the $Mo_2O_4(C_2O_4)_2(H_2O)_2^{2-}$ ion in oxalate solutions at potentials negative of the reduction wave gave irreproducible results. The number of equivalents passed equaled four after ca. four hours and a substantial cathodic current was still present even though sampled cyclic voltammograms indicated that the well defined $Mo_2(V)$ reduction peak had disappeared. Electrolyses, that were continued until the current attained background levels, consumed variable equivalents (6-10 faradays) and produced a fine brown precipitate. The final pH of such solutions was measured at ca. 7, indicating considerable proton consumption. Coulometric reductions were generally carried out in pH 4.69 solutions to achieve sufficient potential separation from background reduction of protons to hydrogen. Reoxidation of the fully reduced solutions was also irreproducible and failed to regenerate the starting complex. Reduction of the $Mo_2O_4(C_2O_4)_2(H_2O)_2^{2-}$ species is evidently both chemically and electrochemically irreversible producing an uncharacterized brown precipitate.

The irreversible electron transfer properties of the $Mo_2O_4(C_2O_4)_2(H_2O)_2^{2-}$ ion are also evident in the pulse polarograms. The reverse pulse polarograms are split into two distinct portions, similar to those of the $Mo_2(V)$ aquo ion, and the $i^{\ell}_{RP1}/i^{\ell}_{NP}$ ratios are consistent with theory (see Appendix 2) for a totally irreversible electron transfer. The normal pulse limiting current corresponds to an overall four-electron reduction step with a diffusion coefficient of $5.2(\pm 0.7) \times 10^{-6}$ cm^2 s^{-1} in 0.5 ionic strength oxalate buffer. Log plots for the normal pulse polarograms of $Mo_2O_4(C_2O_4)_2(H_2O)_2^{2-}$ at varied pH are shown in Figure 3.7. The Tafel slope is essentially the same at all

Figure 3.7. Normal pulse polarographic log plots for the reduction of $Mo_2O_4(C_2O_4)_2(H_2O)_2^{2-}$ in (●) pH 3.07, (■) pH 3.88 and (▲) pH 4.69 oxalate media adjusted to ionic strength 0.5 with KCl. The pulse width was 48.5 ms and the drop time was 1 s.

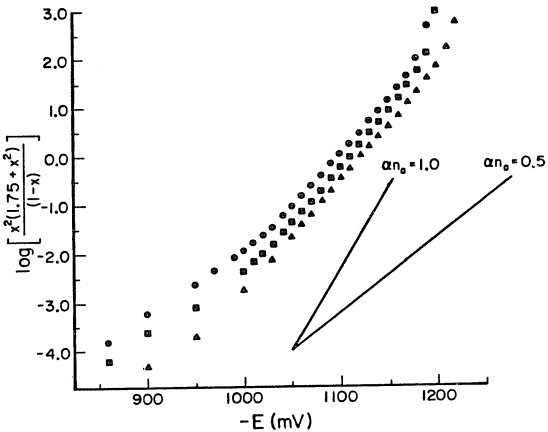
3.0
2.0
1.0
0.0
-1.0
-2.0
-3.0
-4.0
900
1000
1100
1200
-E (mV)
$\log\left[\frac{x^2(1.75+x^2)}{(1-x)}\right]$
$\alpha n_a = 1.0$
$\alpha n_a = 0.5$

three acidities and αn_a is determined to be 0.70. The half wave potential shifts 15 mV per pH unit, considerably less than that exhibited by the $Mo_2(V)$ aquo ion. The proton reaction order dependence ($\Delta \log x / \Delta \log [H^+]$) is 0.25, also considerably less than that shown by the aquo ion. Since the standard potential is unknown for this complex and appears to be unobtainable due to the chemical instability of the reduced products, k_s could not be evaluated. The chemical instability of the reduced products also prevented an independent determination of α in the usual manner.[14]

Discussion

The solution structures of the initial and final states of the $Mo_2(V)/Mo_2(III)$ redox couple were discussed in Chapter 1. The $Mo_2(V)$ aquo ion has a di-μ-oxo core structure (Figure 1.6A) with a terminal oxo on each molybdenum atom.

Elution studies[18] of the $Mo_2(III)$ aquo ion from cation exchange columns have demonstrated a net charge in solution of +4. The two following dimeric structures of the $Mo_2(III)$ aquo ion are consistent with this observation: i) a di-hydroxy bridged species, $Mo_2(OH)_2(H_2O)_8^{+4}$, or ii) a linear oxo bridge ion, $Mo_2O(H_2O)_8^{+4}$. Since the EXAFS analysis clearly rules out[19] the linear oxo bridge species, the most likely structure is the di-hydroxy species shown in Figure 1.6D. Thus, possible redox pathways to account for the electrochemical results will be assumed to involve species with the structures shown in Figure 1.6A and D. It is clear that proton transfer and possible other chemical rearrangements must accompany the addition of electrons to $Mo_2(V)$ to

produce Mo_2(III). In dissecting the possible rate determining steps of this complex electrode reaction the following analysis utilizes a general scheme of squares[20] in which each electron and proton transfer is assigned an independent pathway as shown in Figure 3.8. For simplicity, chemical steps other than proton transfer are neglected, but in principle, they could be easily included in this scheme.

From inspection of Figure 3.8 a multitude of possible pathways link the initial and final states of a general redox sequence involving m electrons and n protons. Proton transfers to oxygen and nitrogen bases in aqueous solution in cases where the free energy is favorable ($\Delta G \leq 0$) have been measured at close to diffusion controlled rates.[21] Under such conditions coupled electron-proton transfers are generally observed, as in the reduction of organic molecules[20] (e.g., quinone). Mathematical descriptions of complex electrode processes such as those for the case $m = n = 2$ have appeared.[20] For the Mo_2(V)/Mo_2(III) redox couple the electrode reaction is sufficiently complex that an exact mathematical explication of all of the possible redox pathways has not been attempted. However, the electrochemical data and chemical intuition allow a delineation of the likely pathways involved in proceeding from Mo_2(V) to Mo_2(III) and vice versa.

For the Mo_2(V) aquo ion two possible rate determining steps appear as likely candidates in the overall reduction to Mo_2(III). Equations (3.6) and (3.7) represent two alternatives that are consistent with the observed value of $\alpha n_a = 0.73$ and the proton reaction order dependence of 1.4.

Figure 3.8. The scheme of squares for an overall m electron - n proton electrode reaction (see text).

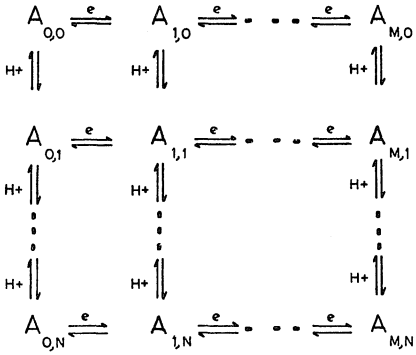

$A_{0,0}$ = $\left[O{=}Mo(O)_2Mo{=}O \right]^{2+}$

$A_{4,6}$ = $\left[Mo(OH)_2Mo(OH)_2 \right]^{4+}$

$$Mo_2O_4(H_2O)_8^{2+} + e + H^+ \xrightarrow[k_f]{r.d.s.} \left[Mo_2O_3(OH)(H_2O)_8^{2+}\right]^{\ddagger} \xrightarrow{3e,\ 5H^+} Mo_2(OH)_2^{4+} \quad (3.6)$$

$$Mo_2O_4(H_2O)_8^{2+} + 2e + 2H^+ \xrightarrow[k_f]{r.d.s.} \left[Mo_2O_3(H_2O)_9^{2+}\right]^{\ddagger} \xrightarrow{2e,\ 4H^+} Mo_2(OH)_2^{4+} \quad (3.7)$$

The electrochemical evidence strongly suggests that the reoxidation of Mo_2(III) to Mo_2(V) is preceded by a rate determining proton dependent step. Deprotonation of coordinated water molecules to form terminal oxo or hydroxyl groups is a plausible interpretation (equation 3.8).

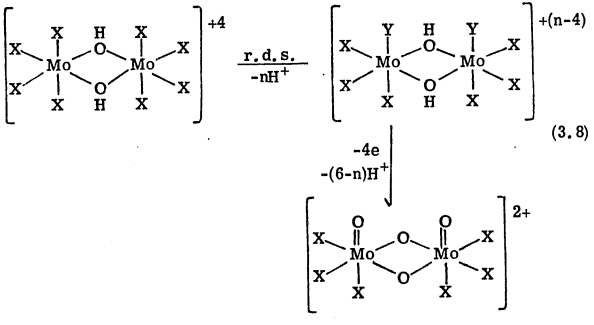

(3.8)

(X = H_2O; Y = OH^- or O^{2-})

However, there is no evidence to rule out alternative chemical rearrangements of the Mo_2(III) species involving the bridging oxygen atoms which

impede the reoxidation to $Mo_2(V)$. The observed reduction and oxidation pathways of the $Mo_2(V)/Mo_2(III)$ redox couple are clearly quite different and are not necessarily the microscopic reverse of one another because of the different possible pathways connecting the two states (Figure 3.8). Oxidation of the monomeric Mo(III) aquo ion to monomeric Mo(V) aquo ion (which dimerizes to form $Mo_2(V)$) is also kinetically limited[5] perhaps because of a deprotonation step to form a terminal oxo or hydroxyl group prior to electron removal.

Essentially identical Tafel slopes are observed for the reduction of $Mo_2O_4(C_2O_4)_2(H_2O)^{2-}$ and the $Mo_2(V)$ aquo ion. The equality of αn_a for the two oppositely charged species suggests a common electron transfer route for reduction.

The proton reaction order for the reduction of the oxalate ion is 0.25, considerably smaller than that for the aquo ion. Similar proton reaction orders have been observed[15] in the reduction of $Mo_2O_4(cys)_2^{2-}$ (cys = cysteine) which also shows a dependence on the total buffer concentration. This point was not addressed in the case of the oxalate ion.

Chemical irreversibility is also clearly evident in the reduction of $Mo_2O_4(C_2O_4)_2(H_2O)_2^{2-}$, a feature that has been previously observed[15] in the four-electron reduction of $Mo_2O_4(cys)_2^{2-}$. In comparison, the four-electron reduction[17] of $Mo_2O_4(edta)^{2-}$ is chemically reversible. In accounting for the chemical stability of the two species the authors[15] could not ascertain whether sulfur bonding by the cysteine ligand labilized the $Mo_2O_4^{2+}$ core or ligand encapsulation by edta stabilized the $Mo_2O_4^{2+}$ core. It seems clear from the reduction of $Mo_2O_4(C_2O_4)_2(H_2O)_2^{2-}$ that stabilizing the $Mo_2O_4^{2+}$ core requires a ligand, such as edta, that effectively protects the bridging oxygens and prevents core breakup.

References and Notes

1. Koval, C., Ph.D.Thesis, California Institute of Technology, 1979.
2. Ichikawa, M. and Meshitsuka, S., J. Am. Chem. Soc., 1973, 95, 3411.
3. Zueva, A. F.; Petrova, G. N.; Efimov, O. N. and Strelets, V. V., Russ. J. Phys. Chem., 1979, 53, 210.
4. Efimov, O. N.; Zueva, A. F.; Petrova, G. N. and Shilov, A. E., Koord. Khim., 1976, 2, 62.
5. Chalilpoyil, P. and Anson, F. C., Inorg. Chem., 1978, 17, 2418.
6. Armstrong, F. A. and Sykes, A. G., Polyhedron, 1982, 1, 109.
7. Spittle, H. M. and Wardlaw, W., J. Chem. Soc., 1928, 2742.
8. Matsuda, H., Bull. Chem. Soc. Japan, 1980, 53, 3439.
9. Oldham, K. B. and Parry, E. P., Anal. Chem., 1968, 40, 65.
10. Delahay, P., "Double Layer and Electrode Kinetics", Interscience, New York, N,Y., 1965, Ch.3.
11. Richens, D. T. and Sykes, A. G., Comm. Inorg. Chem., 1981, 1, 141.
12. Ott, V. R. and Schultz, F. A., J. Electroanal. Chem., 1975, 61, 81.
13. Ibid., 1975, 59, 47.
14. Bard, A. J. and Faulkner, L. R., "Electrochemical Methods", John Wiley and Sons, New York, N.Y.,1980, p. 108.
15. Ardon, M., and Pernick, A., Inorg. Chem. 1974, 13, 2275.
16. a) Chapter 1; b) Lee, P. A., Phys. Rev., 1976, B13, 5261.
17. Albery, W. J. and Hitchman, M. L., "Ring-Disc Electrodes",

Oxford University Press, London, 1971, Ch. 7.

18. Eigen, M., Angew. Chem., 1963, 75, 489.

CHAPTER 4

The Electrochemistry of Trinuclear Aquo Mo(IV) and an Oxalato Derivative in Acidic Media[1]

Introduction

Notable discrepancies regarding solution structure have appeared in the published research on aquo Mo(IV). Souchay and co-workers,[2] in the initial synthesis of aquo Mo(IV), postulated a monomeric structure. A kinetic study of the equilibration of NCS^- with aquo Mo(IV) led Sykes et al.[3] to favor a monomeric formulation, MoO^{2+} (or possibly $Mo(OH)_2^{2+}$). In a later report Ardon and coworkers[4] disproved this assignment when they demonstrated that several species are present when aquo Mo(IV) is equilibrated with NCS^-. From their acid cryoscopy measurements[4] and the ion exchange behavior,[5] they concluded that aquo Mo(IV) exists as a dimeric ion with the probable structure shown in Figure 4.1A. Further support for the dimeric ion came from the initial EXAFS study of Cramer and Gray,[6] although the results were somewhat inconclusive as to whether aquo Mo(IV) is dimeric or trimeric in structure. Finally, the dimeric structure was also favored by Chalilpoyil and Anson[7] in an electrochemical study of the aquo Mo(IV) ion. As described in Chapter 1, more recent structural studies show conclusively that aquo Mo(IV) is trimeric[8,9] with the composition $Mo_3O_4^{4+}$ (Figure 4.1B). A re-examination of the electrochemistry of this ion was undertaken to see if it is consistent with the presence of three reducible centers in the ion. While this study was in progress Richens and Sykes reported the results of experiments on aquo Mo(IV) that included some electrochemical measurements.[10,11] Where they overlap, the experimental observations coincide with those described by Richens and Sykes[11] although a different interpretation of some of

Figure 4.1. A) Postulated structure of aquo Mo(IV); B) Actual core structure[9,12] of trimeric Mo_3(IV) complexes.

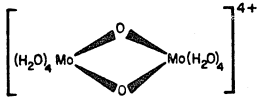

A

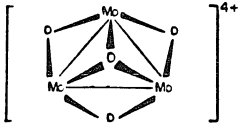

Mo (IV)

B

the electrochemical response exhibited by the aquo Mo(IV) ion will be given.

Experimental

Materials. $Cs_2Mo_3O_4(C_2O_4)_3(H_2O)_3$ was synthesized according to a published procedure.[12] Mo_3(IV) aquo ion was prepared as previously described[7] and further purified by ion exchange on a (Bio-Rad) AG50W-2X cation exchange column (14 × 2 cm). The concentration of Mo_3(IV) was determined by titration with a standard solution of Ce(IV). The molar absorbance of Mo_3(IV) at 508 nm in 2M trifluoromethanesulfonic acid was measured as $\epsilon_{508} = 192\ M^{-1}\ cm^{-1}$ which agreed with a previously reported value[13] in p-toluenesulfonic acid. Solutions of what is almost certainly Mo_3(III) were prepared by controlled potential reduction of Mo_3(IV) at a mercury pool electrode.

Trifluoromethanesulfonic acid, (Minnesota Mining and Manufacturing Co.) was purified by distillation as described in Chapter 2. The concentrated, purified acid was diluted with distilled water that had been further purified by passage through a purification train (Barnstead Nanopure D2790). Stock solutions of lithium trifluoromethanesulfonate were prepared by neutralization of reagent grade Li_2CO_3. Other reagent grade materials were used as received. O-Nitroaniline (Aldrich Chemical Co.) was recrystallized twice. Solutions were deoxygenated by bubbling with pre-purified argon.

Instrumentation and Techniques. Spectra were recorded on Cary 17 or Hewlett-Packard 8450A spectrophotometers. EPR spectra were recorded on a Varian E-Line Century Series spectrometer. Electro-

chemical instrumentation is described in Chapter 2. To permit spectra of air-sensitive electrolysis solutions to be recorded without removal from the electrolysis cell an H-cell with a spectroscopic cuvette attached by an L-shaped arm was constructed. During electrolysis the solution level was below the inlet to the cuvette. To record spectra the cell was tipped to fill the cuvette and the process was reversed when additional electrolysis was desired. Digital simulation of the multiple electron transfer case employed the finite difference equation method of Feldberg[14] (see Appendix 1 for a program listing).

Results

The tris-oxalato complex of Mo(IV). The complete formula of the tris-oxalato complex is $Mo_3O_4(C_2O_4)_3(H_2O)_3^{2-}$.[12] Hereafter we will omit the water molecules in writing the formula of this complex. An earlier polarographic study[15] of the $Mo_3O_4(C_2O_4)^{2-}$ ion reported the presence of two reduction waves but possible structural changes accompanying its reduction were not considered. Cyclic voltammograms of $Mo_3O_4(C_2O_4)_3^{2-}$ exhibit two well-separated reduction steps (Figure 4.2). The separation of the two steps simplifies the interpretation of the behavior of this complex. For this reason we will consider it first because the behavioral pattern it exhibits will prove useful in understanding that of the Mo_3(IV) aquo ion to be described subsequently.

The magnitudes of the cathodic peak currents in Figure 4.2 are consistent with a two-electron step followed by a one-electron step. The first reduction peak is diffusion controlled as determined from the plot of its peak current versus (scan rate)$^{\frac{1}{2}}$ (inset in Figure 4.2). The

Figure 4.2. Cyclic voltammograms of 0.8 mM $Mo_3O_4(C_2O_4)_3^{2-}$ in 0.1 F ($H_2C_2O_4 + K_2C_2O_4$) at pH 1.53. The ionic strength was adjusted to 0.5 M with KCl. Initial potential: -300 mV. Scan rates: 10, 20, 50, 100 and 200 mV s^{-1}. Negative potentials are plotted to the right and reduction currents are plotted upward.
Inset: Peak current vs. $(\text{scan rate})^{\frac{1}{2}}$ for the first cathodic peak.

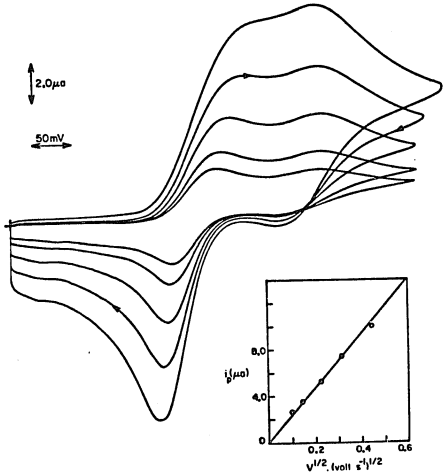
2.0μa
50mV
8.0
4.0
0
0.2
0.4
0.6
$i_p(\mu a)$
$v^{1/2}$, (volt s^{-1})$^{1/2}$

separation between the cathodic and anodic peak potentials of the first wave increases as the scan rate increases as expected if the electrode reaction were only quasi-nernstian. At a scan rate of 10 mV s^{-1} the peaks are separated by 55 mV compared with the 30 mV separation expected for a two-electron nernstian reaction (or the 60 mV expected if the reduction involved only one electron). The second reduction process is also diffusion controlled with an invariant peak splitting of 60 mV. Electrolyte composition had no effect on the peak splitting of the second wave; however, adsorption of the reactant was evident in solutions free of chloride ion. The chloride was added to the supporting electrolyte employed to record Figure 4.2 both to adjust the ionic strength and to suppress this adsorption.

Controlled potential reduction of $Mo_3O_4(C_2O_4)_3^{2-}$ in 0.5 M oxalic acid consumes two faradays per mole of complex when the electrode is held at a potential slightly negative of the first wave (-600 mV). At more negative potentials (e.g., -900 mV) three faradays per mole of complex are consumed. The fully reduced species is stable in the absence of air for at least a week. Its spectrum is shown in Figure 4.3 (curve A) along with that of the original complex (curve C). A spectrum of the two-electron reduction product is also shown in Figure 4.3 (curve B) but the solution also contains a small amount ($\sim$5%) of the fully reduced complex whose formation is difficult to avoid at the potential where the two-electron product is generated at a convenient rate.

The fully reduced ion exhibited the EPR spectrum shown in Figure 4.4A in a frozen solution at 77°K. Solutions of the two-electron reduction product showed essentially no EPR response under the same conditions.

Figure 4.3. Spectra of: A) $Mo_3(OH)_4(C_2O_4)_3^-$; B) $Mo_3(OH)_4(C_2O_4)_3$; C) $Mo_3O_4(C_2O_4)_3^{2-}$ in 0.5 M $H_2C_2O_4$.

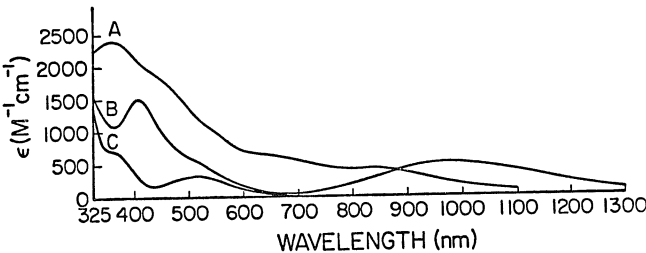
2500
2000
1500
1000
500
0
A
B
C
$\epsilon(M^{-1}cm^{-1})$
325 400 500 600 700 800 900 1000 1100 1200 1300
WAVELENGTH (nm)

Figure 4.4. ESR spectra of: A) $Mo_3(OH)_4(C_2O_4)_3^{=}$; B) Aquo Mo_3(III) ion. Microwave frequencies and modulation amplitudes were A) 9.225 GHz, 1G; B) 9.168 GHz, 2G.

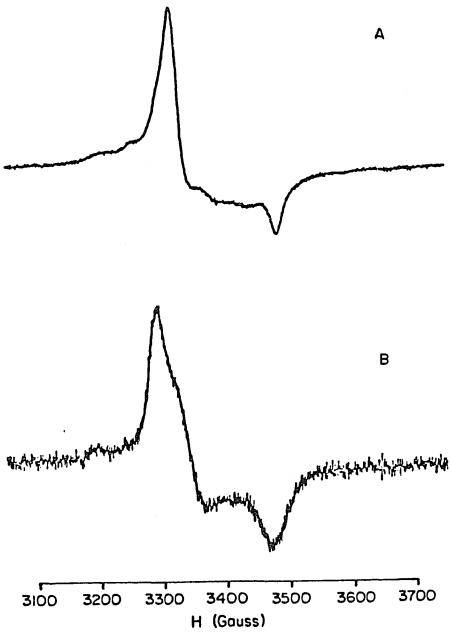
A
B
3100
3200
3300
3400
3500
3600
3700
H (Gauss)

Pulse Polarography. Normal and reverse pulse polarograms[16] for solutions of $Mo_3O_4(C_2O_4)_3^{2-}$ also contain two reduction steps (Figure 4.5). The separation between the two steps is larger in the reverse pulse polarograms (Figure 4.5B) because of the differing electron transfer kinetics exhibited by the two reduction steps: the half-wave potential of the two-electron, quasi-nernstian step is shifted to a more positive value in the reverse pulse polarogram while that of the one-electron nernstian step remains fixed. The two well-developed limiting currents in the reverse polarogram have the expected ratio of 2 to 1. The shapes of the normal and reverse pulse polarographic waves were analyzed by plotting $\log(\frac{i_d-i}{i})$ as a function of the electrode potential.[17,18] The results are shown in curves C and D of Figure 4.5. The slope of the logarithmic plot corresponding to the foot of the first reduction wave is close to 30 mV per decade, as expected for a two-electron reaction. The slope increases as the wave is ascended and the quasi-nernstian character of the wave is expressed. The corresponding plot for the first oxidation wave in the reverse pulse polarogram has a slope near 60 mV over most of the wave as expected for a nernstian one-electron reaction.

The two reduction steps evident in Figure 4.5A are more clearly separated when their derivatives are recorded as in differential pulse polarography.[19] Figure 4.6 shows a set of differential pulse polarograms for a series of $Mo_3O_4(C_2O_4)_3^{2-}$ solutions with varying pH. The peak corresponding to the first two-electron reduction shifts to more negative values as the pH increases until it merges with the second, one-electron peak whose position is insensitive to pH before the merger.

Figure 4.5. Normal (A) and reverse (B) polarograms of 0.8 mM $Mo_3O_4(C_2O_4)_3^{2-}$. Supporting electrolyte as in Figure 4.2. C and D are the corresponding plots of $\log\left(\frac{i_d - i}{i}\right)$ vs. E (see text).

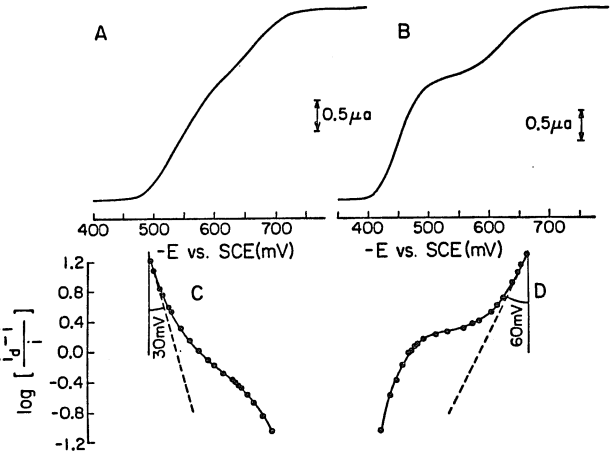
A
B
0.5μa
0.5μa
400
500
600
700
-E vs. SCE(mV)
C
D
30mV
60mV
1.2
0.8
0.4
0.0
-0.4
-0.8
-1.2
log [i_d - i / i]

Figure 4.6. Differential pulse polarograms of $Mo_3O_4(C_2O_4)_3^{2-}$ as a function of pH. All solutions contained 0.1 F total oxalate and the ionic strength was maintained at 0.5 M with KCl. The pH values were: (A) 1.25; (B) 1.57; (C) 1.95; (D) 2.49; (E) 3.05; (F) 3.85; (G) 4.69.

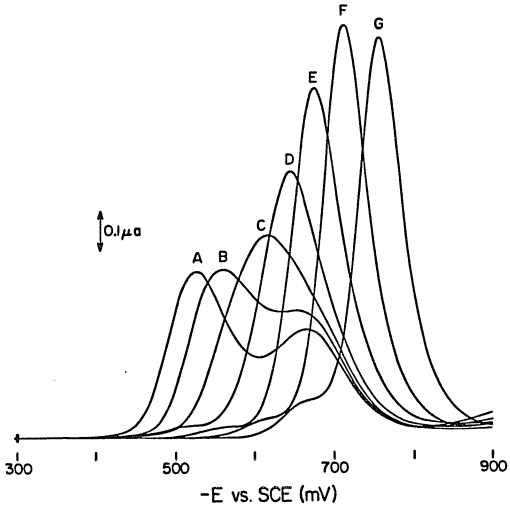
F
G
E
D
C
A
B
0.1μa
300
500
700
900
-E vs. SCE (mV)

The single peak remaining after the reduction steps have coalesced continues to shift to more negative potentials with further increases in pH. (The small wave appearing at the foot of the main waves in Figure 4.6 arose from slight air oxidation of the $Mo_3O_4(C_2O_4)_3^{2-}$ stock solution. The wave is not present in freshly prepared solutions). The peak potentials of the first (or merged) wave in Figure 4.6 are plotted vs. pH in Figure 4.7. At pH values of 2 and below the first wave shifts by 120 mV per pH unit while the peak potential of the coalesced wave shifts by 52 mV per pH unit.

These electrochemical results can be accommodated by the series of electrode reactions depicted in Scheme I:

SCHEME I

$pH < 2$

First step: $Mo_3O_4(C_2O_4)_3^{2-} \underset{-2e^-,\,-4H^+}{\overset{+2e,\,+4H^+}{\rightleftharpoons}} Mo_3(OH)_4(C_2O_4)_3$

quasi-nernstian

Second step: $Mo_3(OH)_4(C_2O_4)_3 \underset{-e}{\overset{+e}{\rightleftharpoons}} Mo_3(OH)_4(C_2O_4)_3^-$

nernstian

$pH > 2$

Two steps merged: $Mo_3O_4(C_2O_4)_3^{2-} \underset{-3e^-,\,-3H^+}{\overset{+3e,\,+3H^+}{\rightleftharpoons}} Mo_3O(OH)_3(C_2O_4)_3^{2-}$

Scheme I implies that one of the oxo-groups in the $Mo_3O_4^{+4}$ core is less basic than the other three and resists protonation in the fully reduced

Figure 4.7. Differential pulse polarographic peak potentials vs. pH for the reduction of $Mo_3O_4(C_2O_4)_3^{2-}$. Conditions as in Figure 4.6.

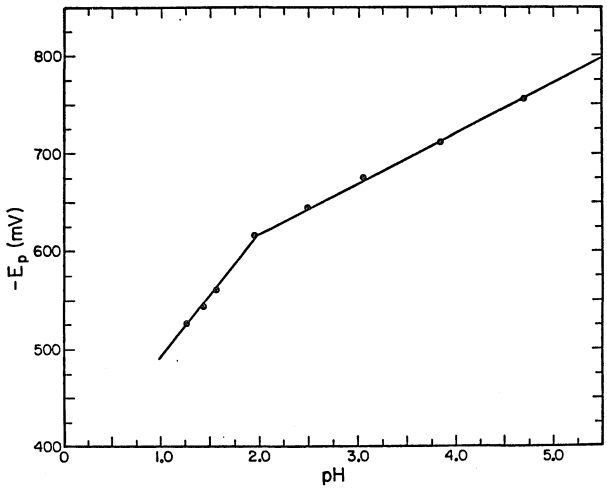
800
700
600
500
400
-Ep (mV)
0
1.0
2.0
3.0
4.0
5.0
pH

ion at pH values above 2. The formal potential of the resulting three electron, three-proton reduction step would be expected to shift by 59 mV per pH unit which is reasonably close to the slope of the line in Figure 4.7 at pH values above 2.

The Aquo $Mo_3(IV)$ Cation. The number of water molecules coordinated to the $Mo_3O_4^{4+}$ core in aquo Mo(IV) has not been determined. On the basis of the known structures of the oxalato and edta complexes[12,20] nine coordinated water molecules seem likely but we will abbreviate the aquo ion as $Mo_3O_4^{4+}$. Cyclic voltammograms of $Mo_3O_4^{4+}$ in a supporting electrolyte composed of 1.0 M trifluoromethanesulfonic acid (HTFMS) and 1.0 M HCl consist of a single reduction and oxidation wave (Figure 4.8). The cathodic peak current increases linearly with $(\text{scan rate})^{\frac{1}{2}}$ (inset in Figure 4.8) and the separation between the peak potentials does not depend on the scan rate. In the absence of chloride less ideal behavior is observed witn unequal anodic and cathodic peak currents.[7] In the presence of chloride, but without explicit electronic compensation to overcome uncompensated resistance in the cell, a separation of 33 mV between the peak potentials was previously interpreted as a sign of a nernstian two-electron reduction.[7] However, a three-electron nernstian reduction in the presence of some uncompensated cell resistance could also have produced a peak splitting in excess of the theoretical value of 20 mV. One purpose of the present experiments was to check this point.

Controlled potential electrolysis of solutions of $Mo_3O_4^{4+}$ at a mercury pool at -500 mV consumes one electron per Mo atom.[7] The

Figure 4.8. Cyclic voltammograms of 0.31 mM $Mo_3O_4^{4+}$. Supporting electrolyte: 1 M HTFMS + 1 M HCl. Initial potential: -100 mV. Scan rates: 10, 20, 50 and 100 mV s^{-1}. Inset: Cathodic peak currents vs. $(\text{scan rate})^{\frac{1}{2}}$. Negative potentials are plotted to the left and reduction currents are plotted upward. Inset: Cathodic peak current vs. $(\text{scan rate})^{\frac{1}{2}}$.

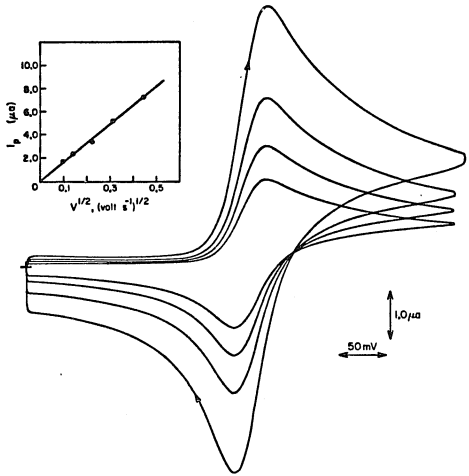
10,0
8,0
6,0
4,0
2,0
0
I_p (μa)
0,1
0,3
0,5
$V^{1/2}$, (volt s^{-1})$^{1/2}$
1,0μa
50mV

resulting complex is readily re-oxidized to $Mo_3O_4^{4+}$ at the electrode or by careful exposure to dioxygen.[10,11] Prolonged exposure of $Mo_3O_4^{4+}$ to dioxygen results in its eventual oxidation to Mo(VI).

Polarography

Normal and reverse (as well as differential) pulse polarograms of solutions of $Mo_3O_4^{4+}$ exhibit only one apparent reduction wave in trifluoromethanesulfonic acid solutions at acid concentrations between 0.5 and 4 M. Figure 4.9 contains representative normal and reverse pulse polarograms. Logarithmic analysis of these two polarograms produced non-linear plots (Figure 4.9, curves C and D). The slopes of the logarithmic plots did not depend upon the duration of the pulses (in the presence of chloride) showing that slow electron transfer was not an important factor.[21] The slopes of the logarithmic plots are consistent with the presence of two successive reduction steps just as was true with the $Mo_3O_4(C_2O_4)_3^{2-}$ complex. However, the two formal potentials for the reduction of the $Mo_3O_4^{4+}$ appear to lie much closer to each other.

A theoretical analysis of the shapes of polarographic waves for overlapping, multi-step, nernstian electrode processes has been presented by Ruzic.[22] This treatment was applied to the case of $Mo_3O_4^{4+}$ by assuming that a two-step reduction involved was analogous to that observed with $Mo_3O_4(C_2O_4)_3^{2-}$ (Reaction 4.1):

$$Mo_3(IV) + 2e \underset{}{\overset{E_1^f}{\rightleftharpoons}} Mo_3(III, III, IV) \qquad (4.1a)$$

$$Mo_3(III, III, IV) + e \underset{}{\overset{E_2^f}{\rightleftharpoons}} Mo_3(III) \qquad (4.1b)$$

Figure 4.9. Normal (A) and reverse (B) pulse polarograms of 0.31 mM $Mo_3O_4^{4+}$. Supporting electrolyte as in Figure 4.8. Parts C and D are the corresponding plots of log $(\frac{i_d - i}{i})$ vs. E (see text).

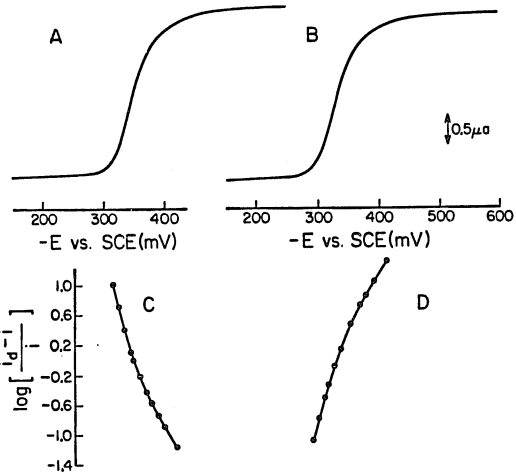
A
B
0.5μa
200
300
400
500
600
-E vs. SCE(mV)
-E vs. SCE(mV)
C
D
log [i_d - i / i]
1.0
0.6
0.2
-0.2
-0.6
-1.0
-1.4

It is convenient to define a comproportionation equilibrium constant relating the three species depicted in equation (4.1).

$$2Mo_3(III) + Mo_3(IV) \rightleftharpoons 3Mo_3(III, III, IV) \qquad (4.2)$$

$$K_c = \frac{[Mo_3(III, III, IV)]^3}{[Mo_3(III)]^2[Mo_3(IV)]} \quad . \qquad (4.3)$$

K_c can also be expressed in terms of the formal potentials of the two redox steps:

$$K_c = \exp\left[\frac{n_1 n_2 F}{RT}(E_1^f - E_2^f)\right] \qquad (4.4)$$

where n_1 and n_2 are the number of electrons involved in the two successive steps. The ratio $(\frac{i_d - i}{i})$ used in the logarithmic analysis of the polarographic wave shapes for this case can be expressed as in equation (4.5).

$$(\frac{i_d - i}{i}) = \frac{1}{p}\left[\frac{\frac{n_2}{n_1+n_2}(K_c p^{n_1})^{\frac{1}{n_1+n_2}} + 1}{\frac{n_1}{n_1+n_2}(\frac{K_c}{p^{n_2}})^{\frac{1}{n_1+n_2}} + 1}\right] \qquad (4.5)$$

where

$$\frac{1}{p} = \exp\{\frac{F}{RT}[(n_1 - n_2)E - n_1E_1^f - n_2E_2^f]\} \qquad (4.6)$$

and E is the potential on the polarographic wave corresponding to each value of i in equation (4.5). Plots of log $(\frac{i_d - i}{i})$ versus E were

calculated from equation (4.5) for several values of $(E_2^f - E_1^f)$ with $n_1 = 2$ and $n_2 = 1$ (reaction 4.1). The results are shown in Figure 4.10 along with the experimental points resulting from the corresponding plot for a normal pulse polarogram of the reduction of $Mo_3O_4^{4+}$. Equation (4.5) produces calculated curves with the same general morphology as the experimental data fall close to the curve calculated for $(E_2^f - E_1^f) = -40$ mV. It is noteworthy that the calculated curves in Figure 4.10 show that clearly non-linear logarithmic plots are to be expected for values of $E_2^f - E_1^f$ as positive as +20 mV. If $(E_2^f - E_1^f)$ is even more positive, linear plots result with slopes corresponding to the sum of n_1 and n_2.

Another useful (but not independent) method for estimating $(E_2^f - E_1^f)$ is to observe the difference in potential between the points where $\log(\frac{i_d - i}{i})$ equals 1.0 and -1.0. An analogous procedure for the analysis of cyclic voltammograms was described by Meyer and Shain.[23] These potential differences (calculated from equation (4.5) are plotted in Figure 4.11 as a function of $(E_2^f - E_1^f)$. When this curve was used to analyze the experimental data shown in Figure 4.10 a value of $(E_2^f - E_1^f)$ of $-(35 \pm 2)$ mV resulted.

Cyclic Voltammetry. The cyclic voltammetric response to be expected from a two-step nernstian electrode reaction that proceeds according to reaction (4.1) can be calculated by means of a digital simulation procedure described recently by Sokol et al..[24] Application of this procedure to the present case (1 M HTFMS + 1 M HCl) gave the best agreement between the experimental and calculated voltammograms with $E_2^f - E_1^f$ set equal to -36 mV (and $n_1 = 2$ and $n_2 = 1$). A comparison

Figure 4.10. Plots of $\log[(i_d - i)/i]$ vs. **E** calculated from equation 5 for different values of $E_2^f - E_1^f$. The experimental points (●) were taken from Figure 4.9C. Values of $E_2^f - E_1^f$ were: (A) +90; (B) +20; (C) 0; (D) -20; (E) -40; (F) -90 mV.

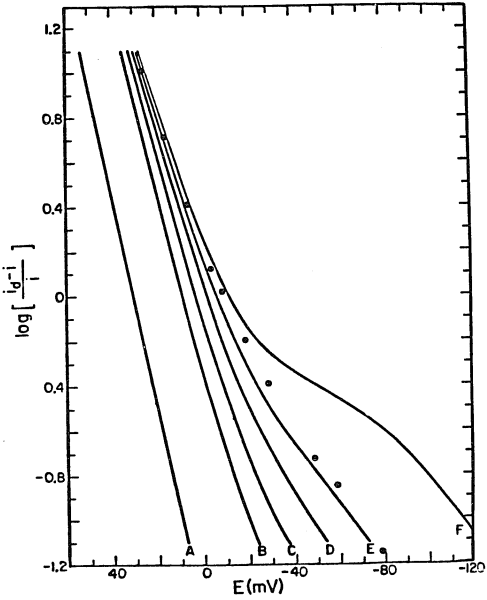
1.2
0.8
0.4
0
0.4
-0.8
-1.2
log [$\frac{i_d - i}{i}$]
40
0
-40
-80
-120
E(mV)
A
B
C
D
E
F

Figure 4.11. Separation in the potentials where $\log\left(\frac{i_d - i}{i}\right)$ equals +1.0 and -1.0 as a function of $E_2^f - E_1^f$. Evaluated from the curves in Figure 4.10.

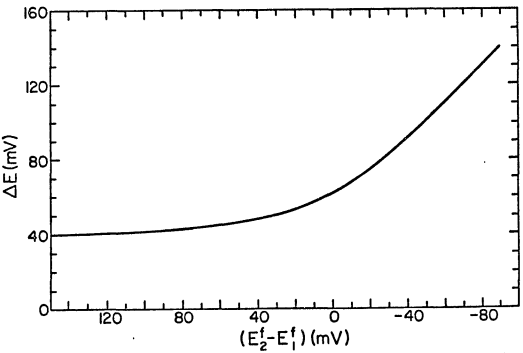
160
120
80
40
0
ΔE (mV)
120
80
40
0
-40
-80
$(E_2^f - E_1^f)$ (mV)

is shown in Figure 4.12A. The agreement is excellent for the cathodic portion of the wave but deviations appear in the anodic portion. The same behavior was also observed by Sokol et al.[24] who attributed them to difficulties in making adequate corrections for the background current during the second half of the cyclic voltammogram. The good agreement we observed for the cathodic portion of the wave adds further support to our supposition that equation 4.1 represents a realistic picture of the pathways involved in the electro-reduction of $Mo_3O_4^{4+}$.

Estimating the closely spaced formal potentials of the multiple electron redox reaction 4.1 from peak separations in the cyclic voltammograms is a rather dubious procedure. Simulated cyclic voltammograms for various values of $(E_2^f - E_1^f)$ (Figure 4.13) show no apparent correlation between cathodic to anodic peak separation and formal potential differences. In fact, the second electron transfer is not readily apparent until the formal potential separation reaches -60 mV.

Acid Dependence of the Half-Wave Potential for $Mo_3O_4^{4+}$ Reduction.

The dependence of $E_{\frac{1}{2}}$ for the composite normal pulse polarographic wave for the reduction of $Mo_3O_4^{4+}$ in solutions containing increasing concentrations of protons is shown in Figure 4.14. The Hammet acidities of each solution, H_0, were evaluated from spectral measurements with o-nitroaniline.[25] The non-linearity of the plot is to be expected if the two steps identified in reaction 1 have different acid dependences. At the lower acidities ($H_0 \leq 0.1$) a limiting slope of ca. 60 mV per H_0 unit results while at higher acidities the slope increases to ca. 90 mV per H_0 unit. These data show that protons are consumed

Figure 4.12. Experimental (solid line) and simulated (points) cyclic voltammograms for $Mo_3O_4^{4+}$. Supporting electrolyte: (A) 1 M HTFMS + 1 M HCl, Scan rate: 200 mV s^{-1}. (B) 2 M HPTS, Scan rate: 50 mV s^{-1}. Initial potential: -100 mV.

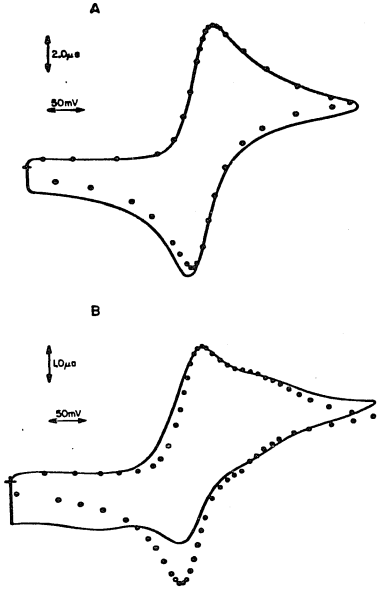
A
2.0μa
50mV
B
1.0μa
50mV

Figure 4.13. Simulated cyclic voltammograms (dimensionless current units) plotted for different values of $E_2^f - E_1^f$ (the cathodic to anodic peak separation is given in parentheses): A) 0 (25) mV; B) -20 (26) mV; C) -40 (31) mV; D) -60 (31) mV; E) -80 (31) mV; F) -100 (31) mV.

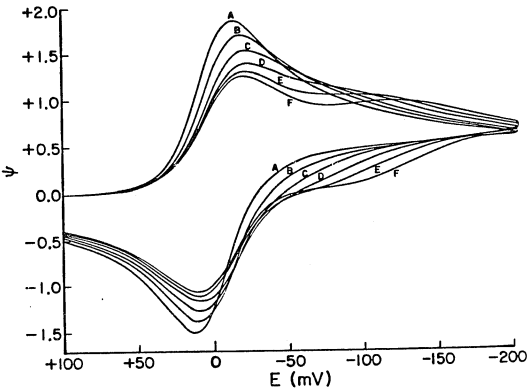
+2.0
+1.5
+1.0
+0.5
0.0
−0.5
−1.0
−1.5
ψ
A
B
C
D
E
F
+100
+50
0
−50
−100
−150
−200
E (mV)

Figure 4.14. Polarographic half-wave potential vs. Hammett acidity function, H_0, for reduction of $Mo_3O_4^{4+}$. Supporting electrolyte: 0.1 M HCl + HTFMS + LiTFMS adjusted to maintain an ionic strength of 2.0 M.

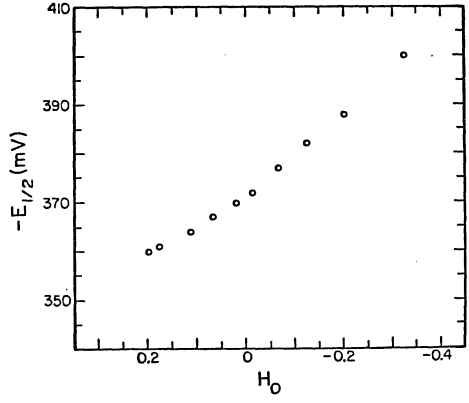
410
390
370
350
$-E_{1/2}$ (mV)
0.2
0
-0.2
-0.4
H_0

in the reduction reaction throughout the range of acidities tested. To dissect the acid dependence into its component parts Figure 4.11 was used to obtain values of $E_2^f - E_1^f$ from the logarithmic analysis of polarograms recorded in solutions of varying acidity. Figure 4.15 displays the log plots obtained at various acidities. (The limits on the range of acidities tested were set on the high side by the desire to maintain constant ionic strength and on the low side by changes in the structure of the $Mo_3O_4^{4+}$ core at acidities below ca. 0.1 M.)[9] A plot of the resulting values of $(E_2^f - E_1^f)$ versus H_0 is shown in Figure 4.16. The data fall on a straight line of slope 43 ± 5 mV per H_0 unit. A number of possible acid dependences of the two reduction steps in reaction 4.1 were considered to account for the slope of the line in Figure 4.16. The closest correspondence results if the first, two-electron step consumes three protons and the second, one-electron step consumes one additional proton as depicted in Scheme II.

SCHEME II

$$\text{First step:}\quad Mo_3O_4^{4+} \underset{-2e,\ -3H^+}{\overset{+2e,\ +3H^+}{\rightleftharpoons}} Mo_3O(OH)_3^{5+} \qquad (E_1^f)$$

$$\text{Second step:}\quad Mo_3O(OH)_3^{5+} \underset{-e,\ -H^+}{\overset{+e,\ +H^+}{\rightleftharpoons}} Mo_3(OH)_4^{5+}$$

The slope of a plot of $E_2^f - E_1^f$ vs. H_0 would be predicted to be 30 mV per H_0 unit on the basis of Scheme II. The observed slope (43 ± 5 mV)

Figure 4.15. Plots of $\log[(i_d - i)/i]$ versus E for different acidities (the ionic strength was maintained at 2.0 by addition of LiTFMS): A) 2.00; B) 1.52; C) 1.12; D) 0.64.

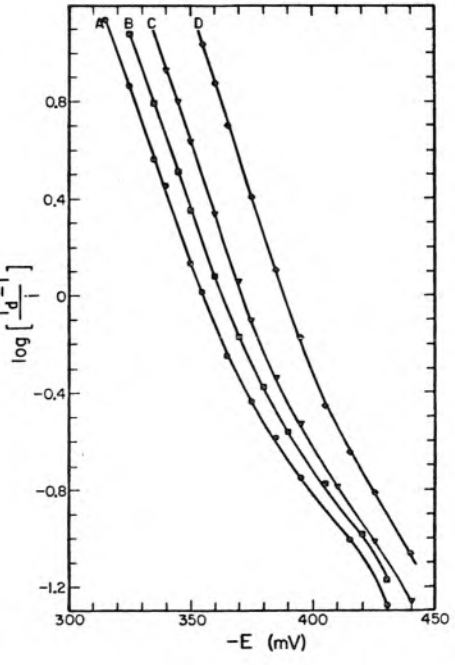
A
B
C
D
0.8
0.4
0
-0.4
-0.8
-1.2
300
350
400
450
-E (mV)
log [i_d - i / i]

Figure 4.16. Values of $E_2^f - E_1^f$ evaluated from Figure 4.11 plotted vs. H_0.

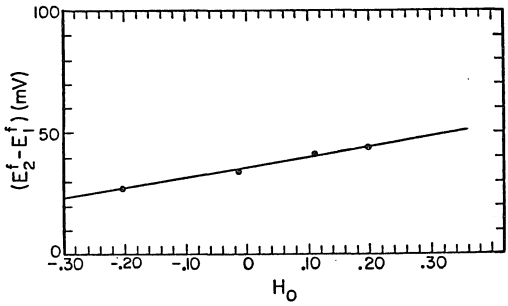
100
50
0
$(E_2^f - E_1^f)$ (mV)
-.30
-.20
-.10
0
.10
.20
.30
H_o

does not seem unreasonable considering the possible sources of error in the many measurements that were required for the preparation of Figure 4.1b.

Absorption Spectra. Uv-visible absorption spectra of solutions containing only $Mo_3(IV)$ or only $Mo_3(III)$ in 0.5 to 4M HTFMS agreed with those reported previously.[10,11] However, similar solutions containing mixtures of these two ions and, therefore, Mo_3(III, III, IV) ion as well, produced somewhat different spectra. To see if this difference was a property of the acidic electrolyte utilized in the previous work (p-toluenesulfonic acid, HPTS), we also recorded spectra of 2:1 mixtures of $Mo_3(III)$ and $Mo_3(IV)$ in this acid. The resulting spectra were identical to those reported previously.[10,11]

p-Toluenesulfonic Acid Media. The dependence of the absorption spectra on the nature of the acid led us to examine the electrochemical behavior of $Mo_3(IV)$ in HPTS. A cyclic voltammogram for $Mo_3(IV)$ in 2M HPTS is shown as the solid line in Figure 4.12B. The presence of two reduction steps is evident indicating that the separation between the formal potentials of the two steps is larger in HPTS than in HTFMS supporting electrolytes. Normal pulse polarograms were recorded in 2M HPTS and their shapes were analyzed by menas of the curve in Figure 4.11 to estimate a 68 mV separation between the formal potentials of the two reduction steps. In 4M HPTS the apparent difference in the two formal potentials increases to ca. 106 mV so that the two stages of the reduction are even more clearly distinguishable. Thus, in HPTS the reduction of $Mo_3(IV)$ appears more similar to that of $Mo_3O_4(C_2O_4)_3^{2-}$ than it does in HTFMS supporting electrolytes.

Estimation of Formal Potentials and Comproportionation Constant. The formal potentials of the half-reactions in Scheme II and the equilibrium constant for reaction 4.2 were estimated at several concentrations of HTFMS from an analysis of the shapes of normal pulse polarograms by means of the curve in Figure 4.11. The resulting values of $E_2^f - E_1^f$ were substituted in equation (4.4) to obtain the values of K_c listed in Table 4.1. The variation of $(E_2^f - E_1^f)$ and, therefore, of K_c with acidity is much smaller than that reported by Richens and Sykes in HPTS electrolytes.[11] As a result, and in contrast with HPTS,[11] reaction 4.2 cannot be forced to proceed completely to the right and the two reduction waves of Mo_3(IV) cannot be completely separated by increasing the concentration of HTFMS. The values of E_1^f and E_2^f in Table 4.1 are similar in magnitude to some of the "reduction potentials" reported by Richens and Sykes but they refer to distinctly different half-reaction for reasons to be discussed.

The aquo Mo_3(III) cation. Cyclic voltammograms for a solution of Mo_3(III) produced by controlled potential reduction of $Mo_3O_4^{4+}$ are shown in Figure 4.17. Two anodic peaks are clearly evident. This contrasts with the anodic response shown in Figure 4.8 during the second half of cyclic voltammograms recorded with solutions of $Mo_3O_4^{4+}$ where only a single anodic peak appears. The implication is that a portion of the Mo_3(III) formed initially from the reduction of Mo_3(IV) undergoes some structural rearrangement on the time scale of controlled potential electrolysis (up to several hours) to produce a form that is re-oxidized at a more positive potential than the unrearranged Mo_3(III). The

Table 4.1. Evaluation of Formal Potentials and the Comproportionation Equilibrium Constant.

$[H^+]$[a] M	$-E_1^f$[b] mV	$-E_2^f$[c] mV	$-(E_2^f - E_1^f)$ mV	K_c[d]
4.10	305	351	46.0	36[e]
2.00	345.5	389	43.5	30
1.52	353.5	395	41.5	25
1.12	364	398	34.0	14
0.64	382.5	409.5	27.0	8

[a]Except for $[H^+]$ = 4.1 M all solutions were prepared from trifluoromethanesulfonic acids, 0.1 M HCl and sufficient lithium trifluoromethanefulfonate to maintain an ionic strength of 2.0 M.

[b]Formal potential of step 1 in Scheme II.

[c]Formal potential of step 2 in Scheme II.

[d]Equilibrium constant for reaction 4.2.

[e]Solution contained only 4.1 M HTFMS.

Figure 4.17. Cyclic voltammograms of $Mo_3(III)$ produced by controlled potential reduction of $Mo_3(IV)$. Supporting electrolyte: 2 M HTFMS. Initial potential: -500 millivolts. Scan rates: 10, 20, 50, 100 and 200 mV s^{-1}. Negative potentials are plotted to the left and reduction currents are plotted upward.

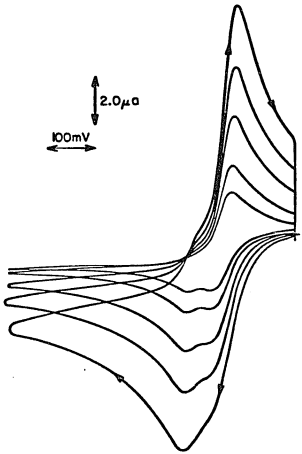
2.0μa
100mV

rearrangement would have to proceed too slowly to be detected by cyclic voltammetry at scan rates as low as 10 mV s^{-1} (Figure 4.8) or reverse pulse polarography with a drop time of 1 sec. (Figure 4.9). To test this supposition solutions of Mo_3(III) were prepared as rapidly as possible by pouring solutions of Mo_3(IV) through a column of zinc metal. (The Zn^{2+} ion introduced into the solution was reduced at potentials outside the range of interest and therefore did not interfere). The resulting solutions were examined periodically by the sensitive method of differential pulse polarography to detect if one or two waves were present in the responses. The results, shown in Figure 4.18, demonstrate that the second wave begins to appear after ca. 2 hours and reaches its final magnitude after ca. 30 hours under the experimental conditions employed. This time dependence of the relative magnitudes of the two waves in solutions containing only Mo_3(III) shows clearly that the species initially formed reacts to produce a more difficultly oxidized form of the same net oxidation state. Since cyclic voltammograms of the solutions showed only a single reduction wave under all conditions, the two forms of Mo_3(III) are apparently oxidized to the single, stable form of Mo_3(IV). This interpretation does not correspond to that proposed by Richens and Sykes who also reported two oxidation waves for Mo_3(III) under some conditions.[10,11] The reasons for this interpretation are given in the Discussion section.

EPR Spectrum of Mo_3(III). Solutions of Mo_3(III) produced EPR spectra such as that shown in Figure 4.4B. The similarity between the

Figure 4.18. Differential pulse polarograms of a solution of MoO_3(III) at various times after its preparation by rapid reduction with zinc metal. The age of the solution was (A) 20 minutes; (B) 8 hours; (C) 12 hours; (D) 22 hours; (E) 36 hours. Initial potential: -550 mV. Between recordings the solution was stirred with argon over a mercury pool maintained at -550 mV.

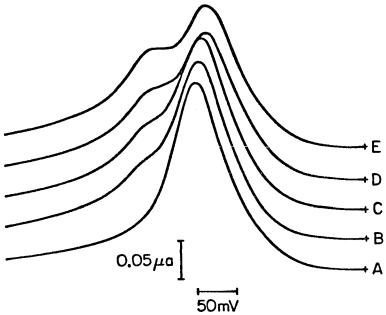
E
D
C
B
A
0.05μa
50mV

spectrum for the aquo and oxalato complexes suggests similar structures for the two ions. Both spectra were eliminated by electrochemical re-oxidation of the reduced ions. When a solution of $Mo_3O_4^{4+}$ in 2M trifluoromethanesulfonic acid was electrolytically reduced by one-third electron per molybdenum atom an EPR spectrum identical to that in Figure 4.4B was obtained but its intensity was only about 10% of that resulting when the electrolysis was carried to completion. The failure of the spectrum's intensity to follow linearly the extent of reduction points to a rapid equilibrium among the various species present with appreciable equilibrium concentrations of all three of the species depicted in Scheme II.

Discussion

Comparison of $Mo_3O_4(C_2O_4)_3^{2-}$ and $Mo_3O_4^{4+}$. The mechanism of the electroreduction of $Mo_3O_4(C_2O_4)_3^{2-}$ is reasonably transparent at acidities where the two reduction steps are well separated. The overall reduction proceeds as indicated in Scheme I. The difference in the pH dependences of the first and second step accounts for the merging of the two waves at pH values above 2.

In solutions of p-toluenesulfonic acid (HPTS) the electrochemical behavior of the aquo Mo_3(IV) cation, $Mo_3O_4^{4+}$, parallels that of the oxalato complex. Adjustment of the formal potentials of the two reduction steps by control of the acid concentration allows large equilibrium concentrations of the partially reduced ion, Mo_3(III, III, IV), to be generated. By contrast, in trifluoromethanesulfonic acid (HTFMS) solutions the smaller separation of the formal potentials for the two

reduction steps of $Mo_3O_4^{4+}$ and their lesser pH dependence leads to much greater disproportionation of the partially reduced ion under all experimentally accessible conditions. This prevented us from using spectral data to evaluate the equilibrium compositions of solutions of Mo(III, III, IV) in HTFMS at any of the concentrations where Richens and Sykes were able to do so in HPTS.[11] The acidities of equally concentrated solutions of HPTS and HTFMS do not differ greatly (as judged from the ratio of protonated to unprotonated o-nitroaniline in the two solutions) so that the difference in the electrochemical responses of $Mo_3O_4^{4+}$ in the two acids probably arises from differences in specific ionic interactions between the molybdenum cations and the PTS^- or $TFMS^-$ anions.

Mo_3(III) Aquo Ion. The pair of anodic peaks in the voltammogram for an aged solution of Mo_3(III) (Figure 4.17) and the single oxidation peak obtained during the oxidizing half of cyclic voltammograms for solutions of Mo_3(IV) (Figure 4.8) clearly point to the occurrence of a chemical reaction subsequent to the electro-reduction of Mo_3(IV). Similar behavior was reported by Richens and Sykes[11] who attributed the double peaks to the existence of two, slowly inter-converting forms of Mo_3(III, III, IV) only one of which could be further reduced to Mo_3(III). The implication was that Mo_3(IV) was reduced only to the irreducible form of Mo_3(III, III, IV) on the time scale of cyclic voltammetry so that only a single reoxidation wave appeared. The longer times involved in controlled potential electrolyses were presumed adequate for some rearrangement of the initially formed Mo_3(III, III, IV) species followed by its further reduction to Mo_3(III). The two waves observed in voltammo-

grams for the oxidation of Mo_3(III) were then presumably ascribed (reference 11 is not explicit on this point) to the formation of the second form of Mo_3(III, III, IV) followed by its further oxidation to Mo_3(IV) without a slow structural rearrangement being required.

This interpretation suffers from the fact that it predicts a voltammetric peak current for the reduction of Mo_3(IV) that corresponds to two rather than three electrons. This is not observed. A further predicted consequence would be a normal pulse polarographic limiting current for the reduction of Mo_3(IV) that is two-thirds as large as that for the oxidation of an equilibrated solution of Mo_3(III). In fact, the limiting currents for these two solutions are virtually identical. Thus, the two forms of Mo(III, III, IV) proposed by Richens and Sykes[11] are not compatible with the observed electrochemical responses.

The most compelling evidence that the chemical transformation involved occurs at the level of Mo_3(III) is contained in Figure 4.18: The second peak in the differential pulse polarogram of solutions of Mo_3(IV) that have been rapidly reduced to Mo_3(III) develops as the fully reduced solution stands. Thus, it appears that two electrochemically distinguishable forms of Mo_3(III) are generated in these solutions. The UV-Vis spectrum of freshly reduced solutions of Mo_3(III) that exhibit just one anodic peak differs only slightly from that of an aged solution that exhibits two peaks (Figure 4.19) and both forms of Mo_3(III) are readily oxidized to the same Mo_3(IV) species. In addition, very slight changes in the EPR signals are observable as the Mo_3(III) solution ages. The structural differences between the two forms of Mo_3(III) (including the possibility that one form may contain more than three Mo atoms)

Figure 4.19. Spectra of $Mo_3(III)$: (A) immediately after preparation; (B) 48 hours later.

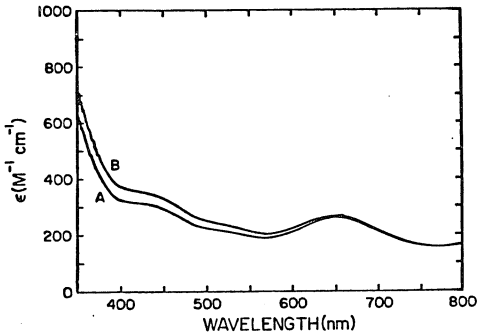
1000
800
600
400
200
0
ε(M⁻¹ cm⁻¹)
B
A
400
500
600
700
800
WAVELENGTH(nm)

remain to be elucidated. However, the existence of two electrochemically distinct forms of Mo_3(III) means that there are two formal potentials connecting the Mo_3(III) and Mo_3(III, III, IV) oxidation states to be considered. The values given in Table 4.1 were obtained under conditions where only freshly formed Mo_3(III) was present so that they represent the formal potential relating Mo(III, III, IV) and that initial form of Mo_3(III). Both the magnitudes and the assignments of the formal potentials given in reference 11 require some revision in the light of these results.

Conclusion

The trinuclear Mo_3(IV) ion is reduced in a two-electron step followed by a one-electron step at potentials that are very close together. The reasons for this reductive pattern are presumably related to structural changes that accompany the reductions. A relevant molecular orbital calculation of Cotton[26] and more recent calculations[27] suggest that the addition of electrons to the $Mo_3O_4^{4+}$ core results in increased electron density on the bridging and capping oxo groups. This is consistent with the coupled electron-proton reduction steps outlined in Schemes I and II in which the formation of hydroxo groups is indicated in the reduced products.

It is interesting to note that molybdenum in oxidation state (III) is now known to form at least three simple aquo ions: Monomeric[28] $Mo(OH_2)_6^{3+}$, dimeric[9] $Mo_2(OH)_2^{4+}$ and the trimeric ion whose core composition is believed to be $Mo_3(OH)_4^{5+}$. In addition, the results presented here indicate that there are two electrochemically distinct forms of the

trimeric ion. Only the trimeric ion is electro-oxidizable to the trimeric molybdenum(IV) ion, $Mo_3O_4^{4+}$. $Mo(OH_2)_6^{3+}$ is electro-oxidized with difficulty[7] and yields the molybdenum(V) dimer, $Mo_2O_4^{4+}$. $Mo_2(OH)_2^{4+}$ is electro-oxidized more readily to the same product.[7] $Mo(OH_2)_6^{3+}$ apparently undergoes slow spontaneous condensation[28] possibly to $Mo_2(OH)_2^{4+}$ but the relative thermodynamic stabilities of the dimeric and trimeric forms of aquo Mo(III) remain to be established.

References

1. This chapter was adapted from a paper in press: Paffett, M. T. and Anson, F. C., Inorg. Chem., 1983.
2. (a) Souchay, P.; Cadiot, M. and Duhameaux, M., C. R. Acad. Sci. 1966, 262, 1524; (b) Souchay, P.; Cadiot, M. and Viossat, B., Bull. Soc. Chim. Fr., 1970, 3, 892.
3. Ojo, J.; Sasaki, Y.; Taylor, R. and Sykes, A., Inorg. Chem., 1976, 15, 1006.
4. Ardon, M.; Bino, A. and Yahav, G., J. Am. Chem. Soc., 1976, 98, 2338.
5. Ardon, M. and Pernick, A., J. Am. Chem. Soc., 1973, 95, 6871.
6. Cramer, S. P.; Gray, H. B.; Dori, Z. and Bino, A., J. Am. Chem. Soc. 1979, 101, 2770.
7. Chalilpoyil, P. and Anson, F., Inorg. Chem. 1978, 17, 2418.
8. Murmann, R. and Shelton, M., J. Am. Chem. Soc., 1980, 102, 3984.
9. Cramer, S.; Eidem, P.; Paffett, M.; Winkler, J.; Dori, Z. and Gray, H., J. Am. Chem. Soc., 1983, 105, 799.
10. Richens, D. and Sykes, A., Inorg. Chim. Acta, 1981, 54, L3-L4.
11. Richens, D. and Sykes, A., Inorg. Chem., 1982, 21, 418.
12. Bino, A.; Cotton, F. and Dori, Z., J. Am. Chem. Soc., 1978, 100, 5252.
13. Richens, D. T. and Sykes, A. G., Comments Inorg. Chem., 1981, 1, 141.
14. Feldberg, S. in "Computers in Chemistry and Instrumentation", Vol. 2 "Electrochemistry", Mattson, J. S.; Mark, H. B., Jr.

and MacDonald, H. C., Jr., Eds., Marcel Dekker, New York, 1972, Chap. 7.

15. Wendling, E. and Rohmer, R., Bull. Soc. Chim. Fr., 1964, 360.
16. Bard, A. J. and Faulkner, L., "Electrochemical Methods", John Wiley and Sons, Inc., New York, N.Y., 1980, p.186.
17. Oldham, K. and Parry, E., Anal. Chem., 1968, 40, 65.
18. Matsuda, H., Bull. Chem. Soc. Japan, 1980, 53, 3439.
19. Reference 16, p. 190.
20. Bino, A.; Cotton, F. and Dori, Z., J. Am. Chem. Soc., 1979, 101, 3842.
21. Fonds, A., Brinkman, A. and Los, J., J. Electroanal. Chem., 1967, 14, 43.
22. Ruzic, I., J. Electronanal. Chem., 1970, 25, 144.
23. Myers, R. and Shain, I., Anal. Chem., 1969, 41, 980.
24. Sokol, W.; Evans, D.; Niki, K.; Yagi, T., J. Electroanal. Chem., 1980, 108, 107.
25. Paul, M. and Long, F., Chem. Revs., 1957, 57, 1.
26. Cotton, F., Inorg. Chem., 1964, 3, 1217.
27. Bursten, B.; Cotton, F.; Hall, M. and Najjar, R., Inorg. Chem., 1982, 21, 302.
28. Bowen, R. and Taube, H., J. Am. Chem. Soc. 1971, 93, 3287.

Appendix 1

Computer Programs

The following programs are listed in order of their appearance in this thesis. With the exception of the simulated cyclic sta case voltammograms of Chapter 2, the programs are self-explanatory and fully referenced in the opening comment statements. The cyclic staircase voltammograms simulated in Chapter 2 were constructed from a simple addition of the current-voltage profiles of the two components computed separately from program SCVNRS.FTN. All programs are written in FORTRAN.

```
C
C PROGRAM SCVNRS
C STAIRCASE VOLTAMMETRY - REVERSIBLE CASE
C FROM PROGRAM BY J. H. CHRISTIE
C
C J TURNER
C 8 AUG 78
C
C MAINLINE PROGRAM
C
      COMMON /BLK1/ F(3000),S(3000)
      COMMON /BLK2/ NFS(10),NTD(10),DE(10),NELEC(10),NPPS(10),
     *DTE(3)
C
C INPUT OF PARAMETERS
C
      CALL SCVNR1(JR)
C
C CALCULATION OF CURRENT FUNCTION
C AND SAVING OF DATA
C
      CALL SCVNR2(JR)
      END FILE 7
      CALL EXIT
      END
```

```
      SUBROUTINE SCVNR1(JR)
      COMMON /BLK1/F(3000),S(3000)
      COMMON /BLK2/NFS(10),NTD(10),DE(10),EI(10),NELEC(10),NPPS(10),
     *DTE(3)
C
C PROGRAM SCVNR5 - SAVES DATA
C SUBROUTINE SCVNR1 - PARAMETER INPUT
C STAIRCASE VOLTAMMETRY - REVERSIBLE REACTION
C FROM PROGRAM BY J. H. CHRISTIE
C DATED 2-18-75
C
C J TURNER
C 30 NOV 77 - MODIFIED 8 AUG 78
C
      WRITE(6,100)
      CALL DATE(DTE)
      WRITE(6,105) (DTE(I),I=1,3)
C
C PARAMETER INPUT SECTION
C
      CALL VARINI (JR,'INPUT NO. OF RUNS ',18,1,10)
      DO 10 JI=1,JR
      WRITE (6,110) JI
3     CALL VARINI(NFS(JI),'NO. OF FORWARD STEPS  ',22,0,400)
      CALL VARINI(NRS,'NO. OF REVERSE STEPS  ',22,1,400)
      CALL VARINI(NPPS(JI),'NO. OF POINTS PER STEP  ',24,1,50)
      NFS(JI)=NFS(JI)+1
      NTD(JI)=NFS(JI)+NRS
      M=NPPS(JI)*NTD(JI)+1
      IF (M.LE.3000) GO TO 5
      WRITE(6,115)
      GO TO 3
5     CALL VARIN(DE(JI),'INPUT STEP HEIGHT - (MV)  ',26,0.1,50.)
      CALL VARIN(EI(JI),'INPUT INITIAL POTENTIAL (MV VS E1/2)  ',38,
     *-1.0E3,1.0E3)
      CALL VARINI(NELEC(JI),'INPUT NO OF ELECTRONS  ',23,1,10)
10    CONTINUE
      RETURN
100   FORMAT (/,' STAIRCASE VOLTAMMETRY - REVERSIBLE REACTION',//)
105   FORMAT ('$ DATE OF CALCULATION ',3A4)
110   FORMAT (/,' FOR PARAMETER SET NO. 'I4)
115   FORMAT (//,' TOO MANY POINTS !!',/)
      END
```

```
      SUBROUTINE SCVNR2(JR)
      COMMON /BLK1/F(3000),S(3000)
      COMMON /BLK2/NPS(10),NTD(10),DE(10),EI(10),NELEC(10),NPPS(10),
     *DTE(3)
      DIMENSION CURR(500)
C
C PROGRAM SCVNRS - SAVES DATA
C SUBROUTINE SCVNR2 - CALCULATION ROUTINE
C STAIRCASE VOLTAMMETRY - REVERSIBLE REACTION
C FROM PROGRAM BY J. H. CHRISTIE
C DATED 2-18-75
C
C J TURNER
C 30 NOV 77 - MODIFIED 8 AUG 78
C
      DEFINE FILE 7(10,1023,U,NXT)
      NXT=1
C
C DEFINITION OF CONSTANTS
C
      NAME=2HNR
12    PI=3.141593
      DO 50 JI=1,JR
      WRITE(6,120) JI
      ANST=3.89232E-2*NELEC(JI)
      CO=2./SQRT(FLOAT(NPPS(JI)))
      LP1=NPPS(JI)+1
      M=NPPS(JI)*NTD(JI)+1
C
C SOLVES THE INTERGRAL USING THE STEP FUNCTION METHOD
C AS EXPLAINED BY NICHOLSON AND OLMSTEAD
C IN ELECTROCHEMISTRY MATTSON, MARK & MACDONALD ED
C CHAPTER 5 PG 127
C
C CALCULATION OF S ARRAY
C
      TEMP=0.
      DO 15 I=1,M
      SQ=SQRT(FLOAT(I))
      S(I)=SQ-TEMP
      TEMP=SQ
15    CONTINUE
C
C SOLUTION SECTION
C
      F(1)=0.
      N=NTD(JI)
      DO 30 I=1,N
      IM1=I-1
```

```
      LAMB=-IM1
      IF(I.GT.NFS(JI)) LAMB=I+1-2*NFS(JI)
      PO=EI(JI)+LAMB*DE(JI)
      EPSP1=1.+EXP(ANST*PO)
      DO 20 K=1,LP1
      M=NPPS(JI)*IM1+K-1
      SM=0.
      DO 25 J=1,M
25    SM=SM+F(J)*5(M-J+2)
      TEMP=(PI/(CO*EPSP1))-SM
      F(M+1)=TEMP
      IF (K.EQ.LP1)CURR(I)=TEMP
20    CONTINUE
30    CONTINUE
      WRITE(7'NXT) NAME,NFS(JI),NTD(JI),DE(JI),EI(JI),NELEC(JI),NPPS(JI)
     *DTE,CURR
50    CONTINUE
      RETURN
120   FORMAT (/,' COMPUTING PARAMETER SET NO. 'I4)
      END
```

```
C PROGRAM TOME
C COMPUTES I/ID AND LOG[ID-I/I] PLOTS FOR
C SEQUENTIAL ELECTRON TRANSFERS
C EE CASE
C SEE I. RUZIC, J. ELECTROANAL. CHEM., 25, 144, (1970).
C PROGRAMMED BY MARK PAFFETT 4/82
C
      DIMENSION EAP(601), CURR(601), TOME(601)
C
C INPUT PARAMETERS
C
      CALL VARIN(A,'INPUT NO. ELECTRONS 1ST STEP ',30,1.,10.)
      CALL VARIN(B,'INPUT NO. ELECTRONS 2ND STEP ',30,1.,10.)
5     WRITE(6,100)
      EPD1=0.0
      CALL VARIN(EPD2,'INPUT POTENTIAL (MV) 2ND STEP ',30,-100.0,100.0
      ANST=3.89256E-2
      LIMIT=601
      AB=A+B
      CK=EXP((A*B*(EPD1-EPD2))*ANST)
      BAP=+150.5
      WRITE(6,105)
      DO 95 I=1,LIMIT
      BAP=BAP-0.5
      EAP(I)=BAP
C
C COMPUTE LOG[ID-I/I] PROFILE
C
      TRIP=EXP(AB*ANST*(BAP-((A/AB)*EPD1)-((B/AB)*EPD2)))
      TRIK=1.0/TRIP
      TRE=CK*(TRIK**A)
      SRE=TRE**(1./AB)
      TOP=((B/AB)*SRE)+1.0
      BRE=CK/(TRIK**B)
      ARE=BRE**(1./AB)
      BOT=((A/AB)*ARE)+1.0
      TOPE=TRIP*(TOP/BOT)
C
C COMPUTE I/ID PROFILE
C
      TRU=(CK*(TRIP**B))**(1.0/AB)
      TRV=((A/AB)*TRU)+1.0
      BRV=TRIP+TRU+1.0
      VRD=TRV/BRV
      CURR(I)=VRD
      TOME(I)=ALOG10(TOPE)
95    CONTINUE
      WRITE(6,110)CK
      WRITE(6,112)
      WRITE(6,115) ((EAP(I),CURR(I),TOME(I)),I=1,LIMIT)
100   FORMAT(1X,'1ST POTENTIAL SET TO 0.0 MV ',//)
105   FORMAT(1X,'E APPLIED STARTS +150 MV FROM EPD1 ',//)
110   FORMAT(1X,' CK = ',E12.6,//)
112   FORMAT(5X,' E APPLIED ',15X,' I/ID ',15X,'LOG[ID-I/I]',//)
115   FORMAT(3X,E16.8,6X,E16.8,6X,E16.8)
      END
```

```
C
C PROGRAM CVRR
C CYCLIC VOLTAMMETRY - MULTISTEP ELECTRODE REACTION
C PROGRAM SUPPLIED BY D.H. EVANS
C SEE J. ELECTROANAL. CHEM.,10B,107-115 (1980)
C MARK PAFFETT 4/82
C
      DIMENSION UB(500),U1(500),U2(500),U3(500)
      DIMENSION CHISV(500),PDTSV(500)
C
C INPUT OF PARAMETERS
C
      CALL VARIN(TEMP,' TEMP (C.) = ',14,0.0,100.0)
      RTF=25.69*(273.15+TEMP)/298.15
      CALL VARIN(EIMV,' INIT POT WRT ED1 = ',21,-1.E3,1.E3)
      CALL VARIN(SWMV,' SWITCH POT WRT TO ED1(MV) = ',29,-1.E3,1.E3)
      CALL VARIN(EED,' ED2 WRT ED1(MV) = ',20,-1.E3,1.E3)
      CALL VARIN(ECD,' ED3 WRT ED1(MV) = ',20,-1.E3,1.E3)
      CALL VARIN(SCANP,' SCANP = FV/RT = A = ',22,-1.E1,1.E1)
C
C SETUP
C
      PNA=EIMV/RTF
      PNB=(EIMV-EED)/RTF
      PNC=(EIMV-ECD)/RTF
      PMOVE=0.0
      THAIN=EXP(-PNA)
      THBIN=EXP(-PNB)
      THCIN=EXP(-PNC)
      MTREV=(SWMV-EIMV)/(RTF*SCANP)
      MAXTT=2*MTREV
      TTMAX=MAXTT
      D=0.45
      NVEMX=6.0*SQRT(D*TTMAX)+2.0
      CHIAT=0.0
      PDTMV=0.0
      SCANF=SQRT(ABS(SCANP*D))
      NPTS=200
      NSAVE=MAXTT/NPTS+1
      MM=0
C
C CLEAR ARRAYS
C
      DO 200 I=1,NVEMX
      UB(I)=0.0
      U1(I)=0.0
      U2(I)=0.0
200   U3(I)=1.0
```

```
C
C SOLUTION SECTION-FINITE DIFFERENCE EQUATIONS
C FELDBERG'S METHOD
C
      DO 800 NTU=1,MAXTT
      TT=NTU
      IF(NTU-MTREV) 220,210,220
210   SCANP=-SCANP
220   CONTINUE
      UU01=U0(1)
      UU11=U1(1)
      UU21=U2(1)
      UU31=U3(1)
      UU02=U0(2)
      UU12=U1(2)
      UU22=U2(2)
      UU32=U3(2)
      PMOVE=PMOVE+SCANP
      SHIFT=EXP(-PMOVE)
      THETA=THAIN*SHIFT
      THETB=THBIN*SHIFT
      THETC=THCIN*SHIFT
      GAMA=1.0+THETA+THETA*THETB+THETA*THETB*THETC
      UU30=(UU31+UU21+UU11+UU01)/GAMA
      UU20=UU30*THETA
      UU10=UU20*THETB
      UU00=UU10*THETC
      DD=2.0*D
      Z0=DD*(UU01-UU00)
      Z1=DD*(UU11-UU10)
      Z2=DD*(UU21-UU20)
      Z3=DD*(UU31-UU30)
      NVE=6.0*SQRT(D*TT)+1.0
      U0(1)=UU01+D*(UU02-UU01)-Z0
      U1(1)=UU11+D*(UU12-UU11)-Z1
      U2(1)=UU21+D*(UU22-UU21)-Z2
      U3(1)=UU31+D*(UU32-UU31)-Z3
      DO 400 I=2,NVE
      UU03=U0(I+1)
      UU13=U1(I+1)
      UU23=U2(I+1)
      UU33=U3(I+1)
```

```
      U0(I)=UU02+D*(UU03-2.0*UU02+UU01)
      U1(I)=UU12+D*(UU13-2.0*UU12+UU11)
      U2(I)=UU22+D*(UU23-2.0*UU22+UU21)
      U3(I)=UU32+D*(UU33-2.0*UU32+UU31)
      UU01=UU02
      UU11=UU12
      UU21=UU22
      UU31=UU32
      UU02=UU03
      UU12=UU13
      UU22=UU23
      UU32=UU33
400   UU32=UU33
      ZFAR=Z1+2.0*Z2+3.0*Z3
      CHIAT=ZFAR/SCANF
      IF(NTU/NSAVE*NSAVE-NTU) 800,600,800
600   MM=MM+1
      CHI5V(MM)=CHIAT
      POT5V(MM)=EIMV+PMOVE*RTF
800   CONTINUE
      WRITE(6,850)
850   FORMAT(1K,' CYCLIC VOLTAMMETRY EEE CASE ',//)
      WRITE(6,1000)MM
      WRITE(6,1005)
      DO 900 I=1,MM
900   WRITE(6,1010)POT5V(I),CHI5V(I)
1000  FORMAT(1K,I4,//)
1005  FORMAT(14K,'POTENTIAL',15K,'CHI',//)
1010  FORMAT(10K,E16.8,5K,E16.8)
      END
```

Appendix 2

Measuring Homogeneous Chemical Reactions Following Electrode Reactions by Double Potential Step Chronocoulometry (DPSCC)

In general, DPSCC experiments are performed as follows: For the simple redox scheme (equation A2.1)

$$Ox + ne \overset{E_0}{\rightleftharpoons} Red \qquad (A2.1)$$

the initial electrode potential is posed at a value (E_0) where no faradaic current flows and is stepped to a potential (E_1) sufficient to produce Red at a diffusion controlled rate. After time τ the potential is stepped back to a potential (E_2) necessary to regenerate Ox at a diffusion controlled rate. The charge is monitored as a function of time during both potential steps and the charge-time behavior is described by equations A2.2 and A2.3 which were derived by Christie[1] for the simple electrode reaction (A2.1).

$$Q_F(t \leq \tau) = 2nFAC_0 \sqrt{\frac{D_0 t}{\pi}} + \Delta q_{01} \qquad (A2.2)$$

$$Q_B(t > \tau) = 2nFAC_0 \sqrt{\frac{D_0}{\pi}} \cdot [\sqrt{t} - \sqrt{t-\tau}] + \Delta q_{01} + \Delta q_{12} \ . \qquad (A2.3)$$

The electrochemical variables have their usual meaning and Δq_{01} and Δq_{12} are the values of the charge consumed by the double layer capacitance upon changing potentials from the respective values. It is more convenient to monitor the reverse charge according to equation A2.4.

$$Q'_B(t > \tau) = Q_B(t > \tau) - Q(\tau) = 2nFAC_o \sqrt{\frac{D_o}{\pi}} \cdot [\sqrt{t} - \sqrt{\tau} - \sqrt{t-\tau}] + \Delta q_{12} \tag{A2.4}$$

Equations A2.2 and A2.4 predict that plots of $Q_F(t \leq \tau)$ versus $t^{\frac{1}{2}}$ and and $Q'_B(t > \tau)$ versus $[\sqrt{t} - \sqrt{t-\tau}]$ should be linear. The intercepts, Δq_{o_1} and Δq_{12}, should be equal to the double layer capacitance values determined in the absence of any electroactive material. A key experimental observable is the value of the ratio, $\frac{Q'_B(2\tau)}{Q'_F(\tau)}$, which in the

$$\frac{Q'_B(2\tau)}{Q_F(\tau)} = \left| \frac{|Q'_B(2\tau)| - |\Delta q_{12}|}{Q_F(\tau) - \Delta q_{o_1}} \right| = 2 - \sqrt{2} = 0.5858 \tag{A2.5}$$

absence of adsorption or homogeneous reactions should be 0.5858.

In electrode reactions where following chemical reactions occur, mathematical solutions to the boundary value problem, where they exist, become quite complex. For the simple EC electrode reaction (A2.6)

$$Ox + ne \overset{E_o}{\rightleftharpoons} Red \xrightarrow{k} C. \tag{A2.6}$$

Christie[1] has derive a complex analytical expression for the ratio

$$\frac{Q'_b(2\tau)}{Q_F(\tau)} = 2nFAC_o \sqrt{\frac{D_o}{\pi}} = 1 - \sqrt{2} + \psi(2\tau, k\tau) \tag{A2.7}$$

where the value of $\psi(t, kt)$ for $t = 2\tau$ is given by

$$\psi(2\tau, k\tau) = -\exp(-2k\tau)\left\{\sum_{n=1}^{\infty} \frac{{}_1F_1(n+\frac{1}{2}, n+1, k\tau)}{n!} \cdot \left[\frac{(k\tau)^{n-}}{2}\right.\right.$$

$$\left.\left. + \sum_{i=1}^{n-1} \frac{(k\tau)^{n-i-1}}{2^{i+2}} \cdot \frac{(2n-1)!!}{(2n-2i-1)!!}\right]\right\} \qquad \text{(A2.8)}$$

$$+ \frac{\sqrt{\pi}}{2} \cdot \frac{\operatorname{erf}\sqrt{k\tau}}{\sqrt{k\tau}} \cdot \exp(-k\tau) \cdot \sum_{n=0}^{\infty} \frac{{}_1F_1(n+\frac{1}{2}, n+1, k\tau)}{2^n n!} \cdot (2n-1)!!$$

The function ${}_1F_1(a, b, z)$ is Kummer's confluent hypergeometric function.[1]

For mechanisms where no analytical solution exists digital simulation[2] allows one to compute solutions for the mechanism at hand. Several groups[3,4] have solved the EC mechanism using digital simulation and good agreement exists between the simulation result and the analytical expression (A2.8) for values of the ratio $\frac{Q'_B(2\tau)}{Q_F(\tau)}$.

Figure A2.1 displays the analytical and simulation results in the form of a working curve. Values of k are determined from Figure A2.1 by measuring the experimental values of $Q'_B(2\tau)/Q_F(\tau)$ at various switching times τ. The charge ratios determined by digital simulation in reference 3 were converted to the present format by the following function, where R_Q is the normalized

$$\frac{Q'_B(2\tau)}{Q_F(\tau)} = (1 - R_Q) \cdot 0.5858 \qquad \text{(A2.9)}$$

charge ratio of reference 3 (its significance is poorly defined in reference 3).

Figure A2.1. DPSCC working curve for the simple EC case of equation A2.6, (—) analytical solution, (■) simulation result of reference 3, (o) simulation result of reference 4.

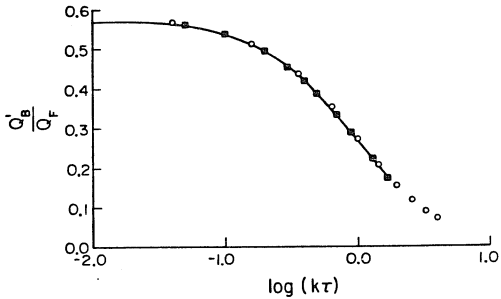
0.6
0.5
0.4
0.3
0.2
0.1
0.0
-2.0
-1.0
0.0
1.0
log (kτ)
Q'B/QF

A similar working curve (Figure A2.2) is derived from the data in reference 3 for reaction A2.10.

$$\begin{aligned} &Ox + ne \overset{E_0}{\rightleftharpoons} Red \\ &2Red \overset{k_d}{\rightleftharpoons} Red_2 \end{aligned} \qquad \text{(A2.10)}$$

The dimerization of monomeric Mo(V) was analyzed from DPSCC data and the working curve of Figure A2.2.

Figure A2.2. DPSCC working curve for the EC radical-radical dimerization mechanism of equation A2.10 (see text).

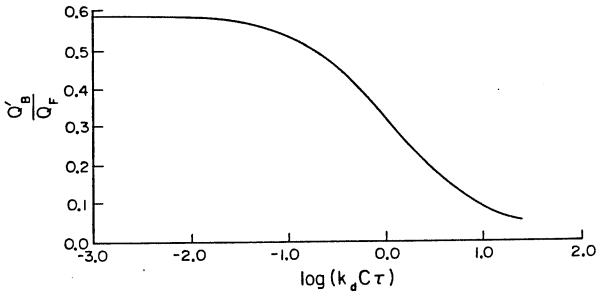
0.6
0.5
0.4
0.3
0.2
0.1
0.0
$\frac{Q'_B}{Q_F}$
-3.0
-2.0
-1.0
0.0
1.0
2.0
log ($k_d C \tau$)

References

1. Christie, J. H., J. Electroanal. Chem., 1967, 13, 79.
2. Britz, D., "Digital Simulation in Electrochemistry", Springer-Verlag, Berlin, 1981.
3. Childs, W. V.; Maloy, J. T.; Kesthelyi, C. P. and Bard, A. J., J. Electrochem. Soc., 1971, 118, 872.
4. Ridgway, T. H.; Van Duyne, R. P. and Reilly, C. N., J. Electroanal. Chem., 1972, 34, 267.

Appendix 3

Normal and Reverse Pulse Polarographic Current-Potential Curves

Pulse polarography utilizes potential pulses applied to a working electrode (DME in this work) and sampling the current just prior to drop dislodgement. Between pulse applications the electrode potential is returned to the initial potential (E_i). The applied potential pulse is linearly increased as a function of time. In normal pulse polarography the initial potential is poised such that no faradaic current flows. For reverse pulse polarography the initial potential is set at a value on the diffusion limited plateau of an electrode reaction and progressively pulsed to a potential where no faradaic current flows in the normal pulse case. A key advantage of pulse polarography is the ability to reduce capacitive charging currents, which decay exponentially, and selectively enhance faradaic currents, which decay according to $E^{\frac{1}{2}}$.

A general theory for pulse polarographic current potential curves has been elegantly derived by Matsuda.[1] The following discussion is a synopsis of the normal and reverse pulse polarographic cases. The current-potential curve for normal pulse polarography is described by equations A3.1-A3.5. The following equations were derived for an initial reduction process as indicated by the superscript c.

$$i^c_{NP} = \frac{(i^c_d)_{cott}}{1 + \exp(\Omega)} \quad , \quad \Phi(\lambda\sqrt{\tau_m}) \tag{A3.1}$$

$$(i^c_d)_{cott} = nFc_o q(t_i + \tau_m)\sqrt{\frac{D_o}{\pi\tau_m}} \tag{A3.2}$$

$$\Phi(\epsilon) = \sqrt{\pi} \cdot \epsilon \cdot F_0(\epsilon) = \sqrt{\pi} \cdot \epsilon \cdot \exp(\epsilon^2)\,\mathrm{erfc}(\epsilon) \tag{A3.3}$$

$$\lambda = \frac{k_f}{D_0^{\frac{1}{2}}} + \frac{k_b}{D_R^{\frac{1}{2}}} \tag{A3.4}$$

$$\Omega = \frac{nF}{RT}(E_2 - E_s) \tag{A3.5}$$

The variable τ_m is the sampling time, E_2 is the potential scanned to, $q(t_1 + \tau_m)$ is the surface area at the DMA evaluated between time t_1 and τ_m and the other variables have their usual meaning. Figure A3.1a displays normalized current potential curves for different values of $\log[k_s\sqrt{\frac{\tau_m}{D_0}}]$. In the case of reversible electron transfer ($k_s \gg 0.01$ cm.sec^{-1}) the polarographic waves are well defined and and traditional log treatments (e.g., $\log[\frac{i_\ell - i}{i}]$ versus E) give linear plots. As the electron transfer becomes less reversible the polarographic wave shape changes and the half-wave potential shifts to values negative of the standard potential. Under conditions where quasi-reversible and irreversible polarograms are obtained the appropriate log plot analysis is given by equations A3.6 and A3.7

$$E_2 = E^* - \frac{RT}{\alpha n_a F} \cdot \ln\left\{x\left[\frac{1.75 + x^2(1 + \exp(\Omega))^2}{1 - x(1 + \exp(\Omega))}\right]^{\frac{1}{2}}\right\} \tag{A3.6}$$

$$E^* = E_s + \frac{RT}{\alpha n_a F} \ln\left[\frac{4}{\sqrt{3}} k_s \sqrt{\frac{\tau_m}{D}}\right] \tag{A3.7}$$

The log plots in Chapter 3 utilize a reduced form of equation A3.6 since under irreversible conditions $\exp(\Omega) \ll 1$.

Figure A3.1. Current-potential curves of a) normal and b) reverse pulse polarography for values of $\log[k_s\sqrt{\frac{\tau_m}{D_o}}]$: 1) ≥ 0.5 (reversible), 2) 0.0, 3) -0.5, 4) -1.0, 5) -1.5, 6) -2.0, 7) -2.5, 8) -3.0.
(Figure taken from reference 1.)

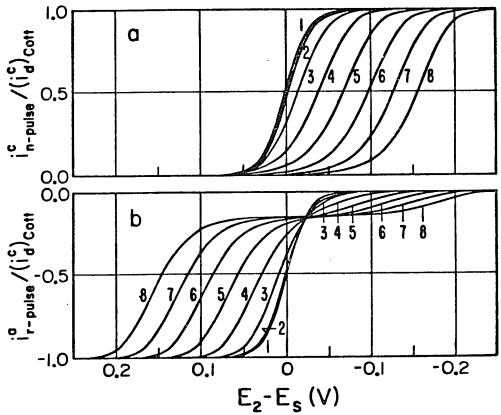
a
b
1.0
0.5
0.0
-0.5
-1.0
0.2
0.1
0
-0.1
-0.2
E_2-E_s (V)
$i^c_{n\text{-pulse}}/(i^c_d)_{Catt}$
$i^a_{r\text{-pulse}}/(i^c_d)_{Catt}$
1
2
3
4
5
6
7
8

The current-potential curve for reverse pulse polarography is described by equations A3.8 and A3.9.

$$i^a_{RP} = \frac{(i^c_D)_{cott}}{1 + \exp(-\Omega)} \cdot \Phi(\lambda\sqrt{\tau_m}) - i^c_{RP1} \cdot F_o(\lambda\sqrt{\tau_m}) \tag{A3.8}$$

$$i^c_{RP1} = \sqrt{\frac{7}{3}}\, nFq(t)C_o\sqrt{\frac{D}{\pi t}}\,. \tag{A3.9}$$

As seen in Figure A3.1b the reverse pulse polarograms for reversible electron transfer have essentially the same shape as the normal pulse polarograms. As the electron transfer becomes less reversible the wave shape changes such that two different limiting currents are observed, i^ℓ_{RP1} and i^ℓ_{RP2}. Under irreversible conditions the limiting current i_{RP1} is given by the Ilkovic equation for instantaneous current (equation A3.9). Although not obvious, the half-wave potential[2] for i_{RP1} lies a few millivolts negative of the half-wave potential for i_{NP}. The ratio of i^ℓ_{RP1} to i^ℓ_{NP} is given by,[2]

$$\left|\frac{i^\ell_{RP1}}{i^\ell_{NP}}\right| = \left[\frac{8t}{7\tau_m}\right] \tag{A3.10}$$

where t is the age of the mercury drop. In addition, the ratio of $(i^\ell_{RP1} + i^\ell_{RP2})$ to i^ℓ_{NP} should be unity in the absence of homogeneous chemical reactions or adsorption processes. The potential of zero faradaic current is obtained in the reverse pulse polarograms on the limiting current plateau i^ℓ_{RP1}. Experimentally, the polarograms in

Chapters 2-4 were displayed in the manner of Figure 3.1b to emphasize the homogeneous chemistry of the participants in the redox reactions.

References

1. Matsuda, H., Bull. Chem. Soc. Jpn., 1980, 53, 3439.
2. Oldham, K. B. and Parry, E. P., Anal. Chem., 1970, 42, 229.